Pliocene–Pleistocene sedimentary development of the syntectonic Polis graben, NW Cyprus: evidence from facies analysis, nannofossil biochronology and strontium isotope dating

Citation for published version:
Balmer, EM, Robertson, AHF, Raffi, I & Kroon, D 2018, 'Pliocene–Pleistocene sedimentary development of the syntectonic Polis graben, NW Cyprus: evidence from facies analysis, nannofossil biochronology and strontium isotope dating', *Geological Magazine*. https://doi.org/10.1017/S0016756818000286

Digital Object Identifier (DOI):
10.1017/S0016756818000286

Published In:
Geological Magazine

Geol. Mag.: page 1 of 29 © *Cambridge University Press 2018*
doi:10.1017/S0016756818000286

Pliocene–Pleistocene sedimentary development of the syntectonic Polis graben, NW Cyprus: evidence from facies analysis, nannofossil biochronology and strontium isotope dating

ELIZABETH M. BALMER*†, ALASTAIR H. F. ROBERTSON*, ISABELLA RAFFI‡ & DICK KROON*

*School of GeoSciences, Grant Institute, University of Edinburgh, James Hutton Road, Edinburgh EH9 3FE, UK
‡Dipartimento di Ingegneria e Geotecnologie (InGeo), CeRSGeoUniversità degli Studi 'G. d'Annunzio' di Chieti-Pescara Campus Universitario, via dei Vestini 31 66013 Chieti Scalo, Italy

(*Received* 19 October 2017; *accepted* 19 March 2018)

Abstract – The recently uplifted and exposed Pliocene and Pleistocene sedimentary infill of the neotectonic Polis graben provides an excellent opportunity to understand extensional basin development in a marine setting. Fieldwork, facies analysis and dating using nannofossils and strontium isotopes reveal how the sedimentary conditions evolved during infill of the Polis graben during Pliocene and Pleistocene time, and allow a composite succession for the depocentre to be determined for the first time. Six lithofacies are recognized in the northern Polis graben, allowing evolving palaeoenvironments to be inferred. By the end of Miocene time (Messinian) a major *c.* N–S-trending graben was established; extensional faulting continued during the Pliocene–Pleistocene until recent time. Post-Messinian salinity crisis deposition began with deposition of hemipelagic muds (*c.* 5.08–2.76 Ma), equivalent to the Nicosia Formation. This was followed by upwards incoming of repeated normal-graded bioclastic carbonates (couplets) (*c.* 2.76–1.6 Ma), which are interpreted as age-equivalents of the Athalassa Formation elsewhere in Cyprus. The upwards sudden facies change is explained by tectonically controlled shallowing which enabled neritic carbonate production on the basin margins. The appearance of basement-derived material (e.g. ophiolitic extrusive detritus) in the highest stratigraphic levels of the basin fill in the north (*c.* 1.7–1.6 Ma) reflects onset of rapid surface uplift focused on the Troodos ophiolitic massif. Overall, the syntectonic basin infill appears to document a two-stage, pulsed uplift related to early-stage collision of the African and Eurasian plates in the easternmost Mediterranean region.

Keywords: Pliocene, Pleistocene, Cyprus, Polis graben, sediments

1. Introduction

1.a. Regional tectonic setting of the Polis graben

The island of Cyprus in the easternmost Mediterranean exemplifies the processes and products of tectonic uplift in a setting of incipient continental collision and westwards tectonic escape of Anatolia towards the Aegean region (Şengör, Görür & Şaroğlu, 1985; Armijo *et al.* 1999; McClusky *et al.* 2000). Recent work indicates that the whole of Cyprus, including the Troodos ophiolite in the south and the Kyrenia Range in the north (Fig. 1), uplifted simultaneously during Pleistocene time (Palamakumbura *et al.* 2016). The main driving force in the uplift of Cyprus is widely considered to relate to the collision of the leading edge of the African Plate, represented by the Eratosthenes Seamount, with a subduction zone dipping northwards beneath the Eurasian plate (Fig. 1; Howell *et al.* 2017).

The Eratosthenes Seamount includes Mesozoic sedimentary rocks that are possibly underlain at depth by dense igneous rocks. The seamount is interpreted as being in collision with Cyprus (Kempler & Ben-Avraham, 1987; Ben-Avraham *et al.* 1995; Robertson *et al.* 1995; Robertson, 1998; Kempler, 1998; Vidal *et al.* 2000; Kinnaird, Robertson & Morris, 2011; Kinnaird & Robertson, 2013; Reiche, Hübscher & Ehrhardt, 2016; Palamakumbura *et al.* 2016). Deep-sea drilling has shown that the Eratosthenes Seamount subsided strongly during late Pliocene – Pleistocene time, which has been explained by flexural collapse during attempted subduction beneath Cyprus (Robertson, 1998). Cyprus underwent corresponding regional tectonic uplift during the same general time period (Robertson, 1977*a*; McCallum & Robertson, 1990; Poole & Robertson, 1998).

Based on evidence from its periphery, the uplift of the Troodos ophiolite is inferred to have taken place mainly during late Pliocene (<2.58 Ma) to middle Pleistocene time (McCallum & Robertson, 1990; Poole, Shimmield & Robertson, 1990; Poole & Robertson, 1991; Harrison *et al.* 2013; Main, Robertson & Palamakumbura, 2016). Several authors have suggested that the uplift was tectonically pulsed (McCallum & Robertson, 1990, 1995*a*, 1995*b*; Weber *et al.* 2011).

Recent work on the Kyrenia Range suggests that rapid uplift began at the end of Pliocene or earliest

†Author for correspondence: b7elizabeth@gmail.com

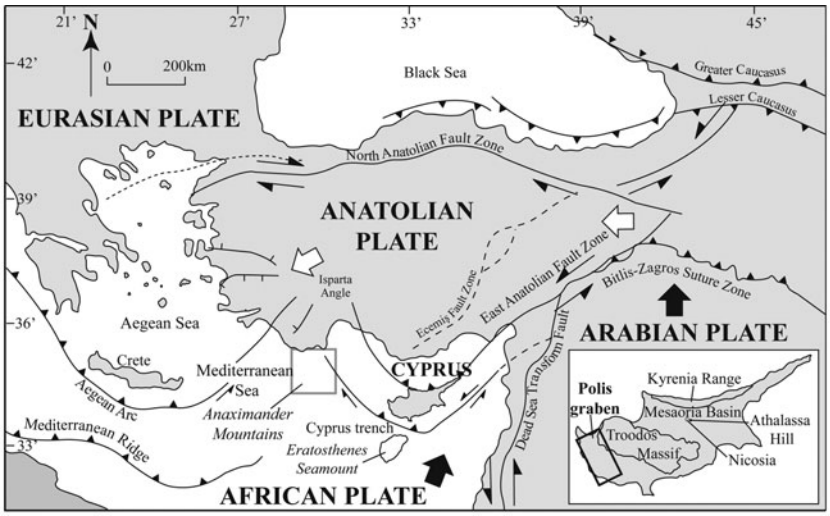

Figure 1. Summary tectonic map of the Eastern Mediterranean region for the Pleistocene Epoch with an inset map of Cyprus. Half arrows indicate directions of regional strike-slip. Barbed lines indicate subduction zones. Large filled arrows indicate convergence directions. Large unfilled arrows indicate regional tectonic escape. The position of the Polis graben is highlighted by the box in the inset map. Modified from McCay & Robertson (2013).

Pleistocene time, with uplift rates peaking during early–middle Pleistocene time (Palamakumbura *et al.* 2016; Palamakumbura & Robertson, 2016).

The Kyrenia Range shows evidence of major southwards thrusting and folding during late Miocene (Messinian) to earliest Pliocene time (Baroz, 1979; Robertson & Woodcock, 1986; McCay *et al.* 2013; McCay & Robertson, 2013). Earlier deformation phases conditioned the crust for further deformation, but are not considered here. The late Miocene – earliest Pliocene compressional deformation is interpreted as the result of the final closure of a second subduction zone which separated the Troodos ophiolite and related crust to the south from the amalgamated Tauride continental crust of Turkey to the north (McCay & Robertson, 2013; Palamakumbura *et al.* 2016, Palamakumbura & Robertson, 2016; Robertson & Kinnaird, 2016).

During and after late Miocene time, much of Cyprus was located in an incipient collisional setting between the sutured African (Arabian) and Eurasian (Tauride) plates to the east in SE Turkey and the open Mediterranean Sea to the SW, represented by the oceanic Herodotus Basin. The palaeo-subduction zone separating North Africa from the Mesozoic crust of Cyprus extended northwestwards to connect with the Cretan arc in the vicinity of the Anaximander Mountains, south of Turkey (Fig. 1; Zitter, Woodside & Mascle, 2003). A contrasting, active plate margin existed to the west of Cyprus during Miocene–Pliocene time. As a result, a fragment of the Mesozoic crust of western Cyprus, represented by Triassic–Cretaceous continental margin and oceanic rocks of the Mamonia Complex and by Late Cretaceous Troodos-type oceanic crust, was able to migrate oceanwards (westwards), opening up a narrow *c.* N–S-trending rift known as the Polis graben (Fig. 1; Elion, 1983; A. Payne, unpub. Ph.D. thesis, University of Edinburgh, 1995).

The Polis graben is inferred to have formed as a result of subduction roll-back and westwards trench migration. Field mapping and measurement of extensional faults indicate that extension took place in an ENE–WSW direction during late Miocene time (Tortonian–Messinian), followed by further extension in a NNE–SSW direction during early Pleistocene time (A. Payne, unpub. Ph.D. thesis, University of Edinburgh, 1995; Payne & Robertson, 1995, 2000; T. Kinnaird unpub. Ph.D. thesis, University of Edinburgh, 2008; Kinnaird & Robertson, 2013).

The Polis graben contributes significantly to an understanding of the geology of Cyprus. In addition, the graben exemplifies structural and sedimentary processes of neotectonic extension and related sedimentation which affected many other areas of the Mediterranean region during Neogene to recent time. Such marine extensional areas include the central Mediterranean (Civile *et al.* 2010), the Aegean region, notably the Gulf of Corinth (Poulos *et al.* 1996; Lykousis *et al.* 2007; Rohais & Moretti, 2017), and the eastern Aegean (e.g. Ocakoğlu, Demirbağ & Kuşçu, 2004). Similar extensional processes and related sedimentary deposits characterize other complex multi-plate regions such as the Caribbean (Driscoll & Diebold, 1999; Escalona & Mann, 2011) and Indonesia, for example Kalimantan Basins, Borneo (Van de Weerd & Armin, 1992; Hall, 2002). Acquiring additional information on the deep sedimentary fill of marine extensional basins requires deep-sea drilling, as recently achieved for the Gulf of Corinth (Greece) (McNeill, Shillington & Carter, 2017) during October–December 2017, together with ongoing onshore studies (January 2018 onwards).

Extensional basins exposed on land typically have a patchy non-marine sedimentary record which is difficult to date accurately, for example the grabens of western Turkey (Yılmaz *et al.* 2000; Purvis

& Robertson 2005*a*, *b*; Çiftçi & Bozkurt, 2009), southern Turkey (Boulton, Robertson & Ünlügenç, 2006; Boulton *et al*. 2007) and northern Syria (Hardenberg & Robertson, 2007). In this regard, the Polis graben represents an exceptional opportunity to understand subaqueous rift-related sedimentation because it developed in a marine environment but was then uplifted and exposed due to the rapid Pleistocene uplift of Cyprus.

1.b. Stratigraphy of the Polis graben

The present study focuses on the Pliocene and Pleistocene sedimentary fill of the Polis graben. However, the preceding geological development is relevant here because older units contributed to the sediment provenance. The outcrop pattern also provides clues to depositional pathways. In general, the Pliocene–Pleistocene sediments occur at relatively low topographical levels within the Polis graben, whereas older units are exposed on the graben flanks and hinterland (Fig. 2a).

The oldest rocks in SW Cyprus are represented by the Mamonia Complex of Triassic–Cretaceous age, which includes a wide range of sedimentary rocks but also basic igneous rocks and sparse metamorphic rocks (Figs 2b, 3; Robertson & Woodcock, 1979; Swarbrick & Robertson, 1980). The Mamonia Complex is exposed widely on the western flank of the Polis graben and patchily in the SW, south and SE (Fig. 3). On both flanks of the Polis graben there are also significantly sized outcrops of large-scale debris-flow deposits, represented by the Upper Cretaceous (Maastrichtian) Kathikas Formation which contains similar lithologies to the Mamonia Complex (Swarbrick & Naylor, 1980). The Polis graben is bounded to the east by the Upper Cretaceous Troodos ophiolite, and there is an additional small ophiolitic outcrop in the NW (Akamas ophiolite). Basaltic extrusives (>250 m thick) are exposed in both ophiolites. Both ophiolites are also overlain by volumetrically minor Upper Cretaceous metalliferous and siliceous sediments (Perapedhi Formation), which pass upwards into widespread outcrops of Upper Cretaceous volcanogenic mudrocks and sandstones (Kannaviou Formation) (Robertson, 1977*b*).

The Polis graben has been divided into southern and northern sub-basins (Payne & Robertson, 1995). This study focuses on the northern sub-basin, north of Polemi (Fig. 2), here termed the 'northern Polis graben'.

In the southern sub-basin, the Upper Cretaceous sediments pass upwards first into Palaeogene pelagic chalks and cherts of the Lefkara Formation, and then into marls, chalks and limestones of the Miocene Pakhna Formation and associated reefal members (Henson, Browne & McGinty, 1949; Follows, Robertson & Scoffin, 1996; Banner, Lord & BouDagher-Fadel, 1999; BouDagher-Fadel & Lord, 2006; Fig. 2b). The Pakhna Formation passes upwards into Messinian gypsum, known as the Polemi basin (Orszag-Sperber, Rouchy & Elion, 1989; Rouchy *et al.* 2001).

In contrast, in the northern sub-basin the Mesozoic lithologies are unconformably overlain by carbonates of the Miocene Pakhna Formation, without preserved Palaeogene pelagic carbonates between (Fig. 2b). Minor non-evaporitic Messinian sediments crop out on both flanks of the northern Polis graben (Kinnaird & Robertson, 2013; this study). Throughout the northern graben, Pliocene sediments overlie the Miocene facies unconformably, wherever exposed (Fig. 2b). The Pliocene lithologies are, in turn, unconformably overlain by Pleistocene non-marine facies inland and by littoral facies near the coast (Chrysochou Bay).

1.c. Outline structure of the Polis graben

The Polis graben is an asymmetrical structural depression that trends NNW–SSE (Fig. 2c; Elion, 1983; A. Payne, unpub. Ph.D. thesis, University of Edinburgh, 1995; Payne & Robertson, 1995, 2000; T. Kinnaird unpub. Ph.D. thesis, University of Edinburgh, 2008; Kinnaird & Robertson, 2013). The graben is bounded to the ENE and WSW by 'first-order' major normal faults, together with 'second-order' block-bounding faults (Fig. 2c; Payne & Robertson, 1995, 2000). Five major normal faults are mapped on the eastern flank, four of which dip at 50–60° to the WSW and one at 50–60° to the ENE. In addition, two major subparallel normal faults are identified on the western flank, striking NNW–SSE (Payne & Robertson, 1995, 2000). Both back-rotated and forward-rotated fault blocks occur on the western flank of the graben. Overall, two phases of faulting are identified: NNW–SSE faults mainly cutting Miocene and older units; and WNW–ESE faults mainly cutting Palaeogene, Miocene and Quaternary units (Payne & Robertson, 1995, 2000; Kinnaird & Robertson, 2013). The combined sedimentary evidence from the Miocene Pakhna Formation and the fault structural evidence indicates that the Polis graben was highly active during late Miocene time (Tortonian–Messinian), providing accommodation space for sediment accumulation (see Section 7.c). The graben is transected by a major transverse (transfer) fault, which created separate northern and southern sub-basins and thereby influenced sediment accumulation and depositional pathways during and after late Miocene time. Recently created outcrops reveal a somewhat more complex pattern of extensional and transverse faults than previously known, which remain to be mapped in detail.

1.d. Pliocene sediments of the Polis graben

The Pliocene outcrop in western Cyprus was initially mapped on the basis of lithological correlation with Pliocene sediments elsewhere in Cyprus, for which preliminary micropalaeontological data indicated a Pliocene age (Henson, Browne & McGinty,

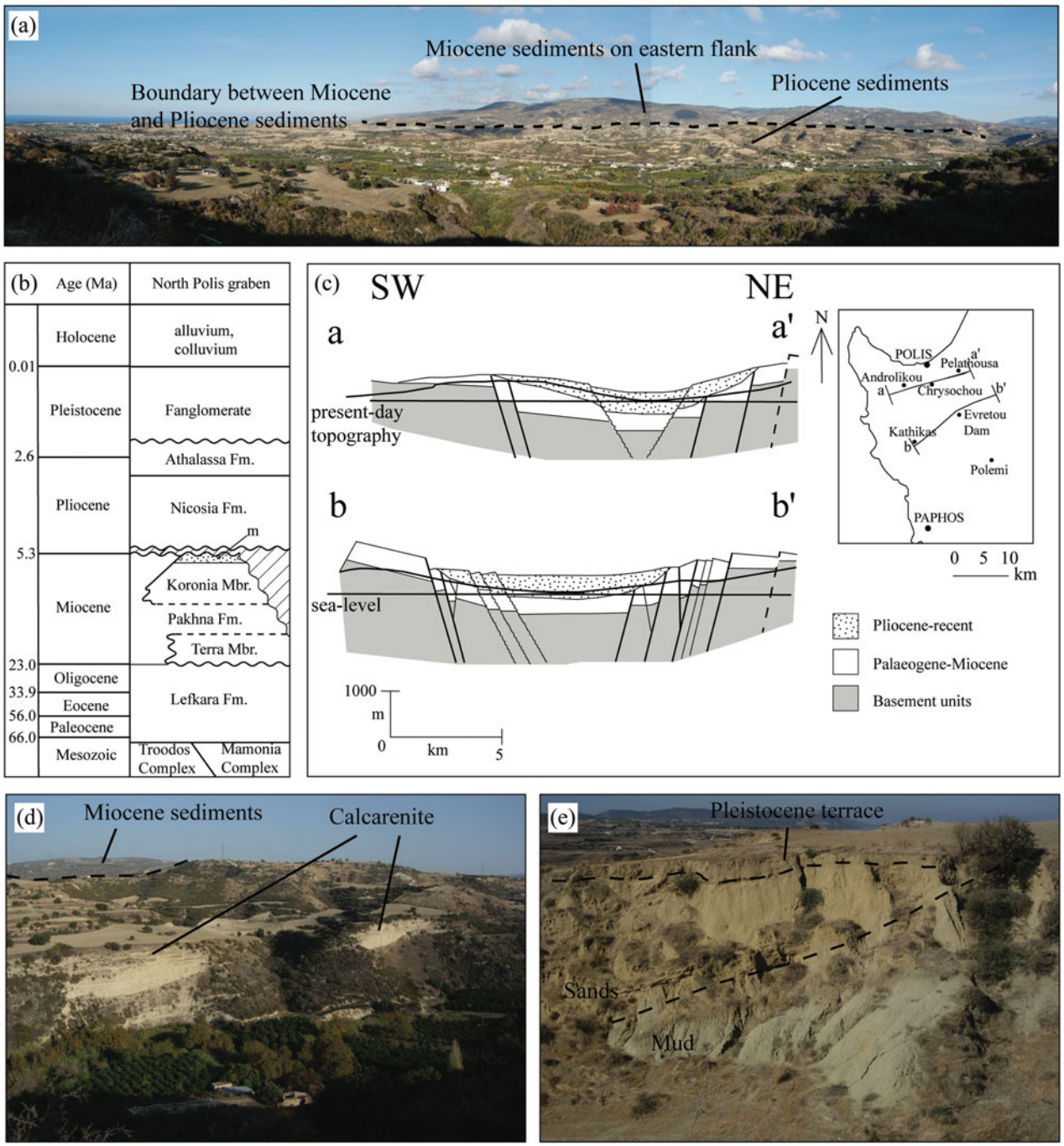

Figure 2. (Colour online) (a) Looking NE across the northern part of the Polis graben, showing the boundary between the Pliocene sediments located near the graben axis and the hilly Miocene outcrop on the eastern flank of the graben. (b) Age and stratigraphy within the northern part of the Polis graben (adapted from Payne & Robertson, 1995), indicating the prior stratigraphy to be tested; m – unnamed Messinian non-marine facies. (c) Structural cross-sections of the Polis graben; thick lines, first-order faults (dashed, inferred); reproduced from A. Payne, unpub. Ph.D. thesis, University of Edinburgh (1995). (d) Hill composed of a thick exposure of Pliocene calcarenite with Miocene sedimentary rocks in the distance. (e) Contact between hemipelagic mudstone and sandstone in the northern, axial part of the Polis graben.

1949; Bear, 1960; Gass, 1960; Baroz, 1979). The Pliocene sequence in the type area, the Mesaoria Basin (Fig. 1), was initially divided into the stratigraphically lower Nicosia Formation and the stratigraphically higher Athalassa Formation. The type area of the Nicosia Formation, around the capital city, is dominated by a *c.* 750 m thick sequence of marls and chalks, whereas the type sequence of the Athalassa Formation near Nicosia (Athalassa Hill) is mainly shallow-water marls and bioclastic limestones (Fig. 1; Henson, Browne & McGinty, 1949). Other formations that are exposed near the Troodos ophiolite in the south are not considered here.

Geological maps of Cyprus distinguish the Nicosia and Athalassa formations throughout Cyprus. However, the distinction between the two formations in

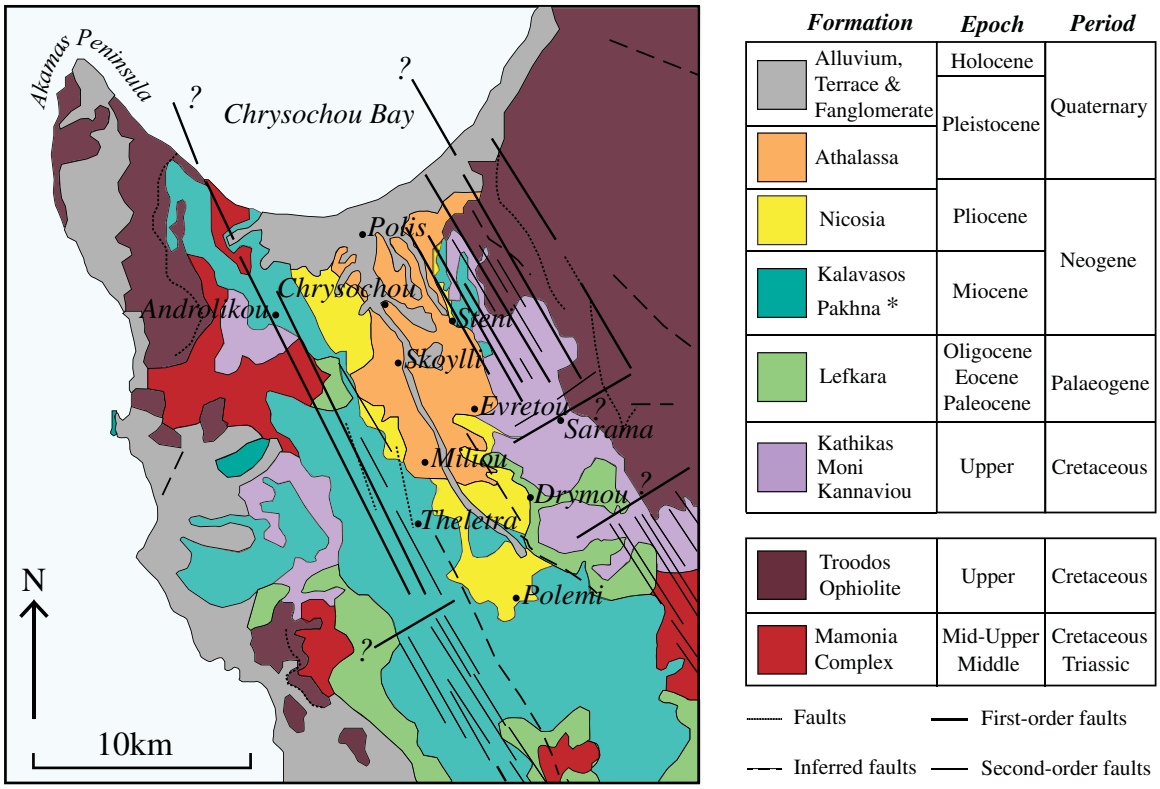

Figure 3. (Colour online) Outline geological map of NW Cyprus based on the 1:250,000 Geological Map of Cyprus, published by the Cyprus Geological Survey Department, Nicosia (Constantinou, 1995) with the faults (dotted line) and inferred faults (dashed line) indicated. The distribution of the Nicosia and Athalassa formations are modified based on this study. (*Pakhna formation includes the Koronia and Terra members.) The simplified first-order (bold line) and second-order (faint line) faults indicated are adapted from A. Payne, unpub. Ph.D. thesis, University of Edinburgh, 1995.

western Cyprus was difficult in the absence of sedimentological or dating evidence. As a result, different generations of maps showed different outcrop patterns, with an earlier map (Pantazis, 1979) showing the Athalassa Formation as cropping out quite far inland within the axial area of the Polis graben. In contrast, a more recent map (Constantinou, 1995) shows the Athalassa Formation as mainly restricted to near Chrysochou Bay in the north (Fig. 3). The contrasting outcrop of the Nicosia and Athalassa formations as implied by the latter study is also shown in Figure 3.

In recent years, information on the age of the Nicosia Formation in the Mesaoria Basin has increased considerably based on micropalaeontology (e.g. Lord, Panayides & Xenophontos, 2000; Harrison *et al.* 2004, 2008, 2013) and magnetostratigraphy (Kinnaird, Robertson & Morris, 2011; Weber *et al.* 2011). In addition, the sedimentology and palaeoenvironments of both the Nicosia Formation (McCallum & Robertson, 1990, 1995*b*; Schirmer *et al.* 2010) and the Athalassa Formation (McCallum & Robertson, 1995*a*; Palamakumbura & Robertson, 2016) have been investigated in some detail, although there is still scope for improved micropalaeontological dating in particular. In contrast, the age and sedimentology of the Pliocene and Pleistocene sediments (Fig. 2d, e) of the Polis graben in western Cyprus have, until now, remained virtually unstudied.

2. Materials and methods

Fieldwork focused on the northern Polis graben, extending from Polemi in the south to Polis in the north (Fig. 3). Sedimentary logs were measured to help determine the lithofacies present within the basin (see Section 3). The biostratigraphic dating was carried out using calcareous nannofossils and strontium isotopic analysis (see online Supplementary Material at http://journals.cambridge.org/geo for GPS locations of samples). In addition, samples were collected for microfacies and provenance analysis.

For the nannofossil biochronology, 38 samples ranging from hemipelagic mudstone to fine sandstone were selected as representative of the main sedimentary sequences that are exposed near the basin axis and from both the eastern and the western flanks of the graben, that is, from both high and low topographic areas.

In addition, 20 samples from the same sample set were selected for $^{87}Sr/^{86}Sr$ isotopic age dating. A mixture of 150 planktonic and benthic foraminifera were handpicked from each sample. The $^{87}Sr/^{86}Sr$ isotopic analysis was carried out at the Scottish Universities Environmental Research Centre (SUERC) in East Kilbride, followed by the calculation of the combined error (see online Supplementary Material at http://journals.cambridge.org/geo for further information).

3. Measured sequences

An overall northwards dip of *c.* 2–12° towards the NNW–NE was measured within the northern Polis graben. The tilting took place after sedimentary infill and resulted in the observed overall northwards younging of the basin. Only thin, local sequences (<10 m) are exposed (Fig. 4). To determine an overall reference succession applicable to the basin axis, the local measured sequences were correlated lithologically where possible. The new nannofossil and strontium isotopic data were used to assemble the logs into an overall chronological order as far as possible. The resulting reference succession (see Section 5) is inferred mainly based on sequences that were measured <2 km from the basin axis. Some local sequences that were measured on the flanks of the graben (e.g. near Pelathousa and Steni) do not fit simply into the reference succession, which reflects facies variation from the basin axis to both flanks of the northern Polis graben.

The measured logs (Fig. 4) encompass a wide range of lithologies. Close to the basin axis hemipelagic mudstones predominate, as exposed in the south (e.g. Fig. 4, logs 2, 3). Calcareous mudstones are typically interbedded with normal-graded calcarenites, here termed couplets, which are mostly exposed near the basin axis (e.g. Fig. 4, logs 6, 8). The thickness of individual couplets varies from <10 cm to 1 m. Some calcarenite beds fine upwards from coarse- to medium-grained calcarenite (e.g. Fig. 4, logs 9, 13), whereas others grade into purer mudstones (e.g. Fig. 4, log 4). The basal part of many individual calcarenite beds contains abundant bioclastic material including bivalves, gastropods and scaphopods (e.g. Fig. 4, log 8). Laminations and vertical burrows are common in some couplets (e.g. Fig. 4, logs 6, 7).

Towards the north, repeated grainstone beds are separated by thin to medium (10–30 cm) interbeds of calcareous mudstone (e.g. Fig. 4, logs 10, 11). The grainstone beds contain bivalves, gastropods and scaphopods. Carbonate concretions occur locally, aligned within and parallel to grainstone beds. Above the mudstones, sandstone beds, which mostly contain bivalve detritus, are common in the north of the area (e.g. Fig. 4, logs 14, 15). In addition, mudstones and siltstones on the flanks of the basin are locally overlain by bivalve-rich carbonate breccia (e.g. Fig. 4, log 17). Also on the graben flanks, mudstones are rarely interbedded with organic-rich layers which contain rootlets, plant material and conglomerate lenses (e.g. Fig. 4, log 16).

4. New dating using nannofossils and strontium isotopes

The Pliocene–Pleistocene boundary is now set at 2.58 Ma (Cohen & Gibbard, 2010), whereas previously it was at 1.8 Ma. As a result, some palaeontologically assigned late Pliocene ages (e.g. Lord, Panayides & Xenophontos, 2000) are now redefined as being of early Pleistocene age.

New nannofossil biochronological data for the 38 selected samples are summarized in Table 1. The resulting age ranges are plotted in Figure 5, where they are compared with the ages obtained from the $^{87}Sr/^{86}Sr$ isotopic dating (including calculated errors). Samples listed as having rare nannofossils or being 'barren' are excluded. The sample numbers are generally arranged from the most northerly sample collected (PL59) to the most southerly sample (PL21). Some of the samples come from the basin flanks, where lithologies differ somewhat from near the basin axis. Age-diagnostic taxa are listed in Table 2. Samples that are 'barren of nannofossils' are omitted. The preservation and abundance of nannofossil assemblages are variable. In some samples *in situ* assemblages are diluted as a result of strong reworking of Cretaceous and Palaeogene taxa and by clay-rich terrigenous input, which preclude accurate biochronology.

The $^{87}Sr/^{86}Sr$ ages obtained for the 20 selected samples are also shown in Table 1. To assign ages for the $^{87}Sr/^{86}Sr$ ratios recorded, the most recent Sr isotopic Look-Up Table was used, that is, Version 4: 08/04 (Howarth & McArthur, 1997; McArthur, Howarth & Bailey, 2001). The specific $^{87}Sr/^{86}Sr$ isotopic ages range from 1.25 Ma to 5.46 Ma with combined errors for these specific ages ranging from 0.86 Ma to 5.92 Ma.

Nineteen samples provided a $^{87}Sr/^{86}Sr$ isotopic date and also a nannofossil age range. Of these 19 samples, 7 of the nannofossil age ranges fall within the strontium isotopic error range (sample numbers: 5, 9, 17, 18, 46, 65, 90) and 6 nannofossil age ranges overlap with the strontium isotopic error range (sample numbers: 3, 11, 12, 15, 21, 66). Overall, the results are coherent with 13 out of 19 samples showing similar age ranges. However, 6 nannofossil age ranges lie outside the strontium isotopic error range (sample numbers: 2, 70, 74, 78, 84, 89). Overall, the nannofossil biochronology was found to provide a higher age resolution than the strontium isotopic data (Fig. 5), and so was used preferentially. The main reasons are that strontium isotope ratios are potentially sensitive to diagenetic changes or subaerial weathering (DePaolo & Ingram, 1985).

The changing slope of the global $^{87}Sr/^{86}Sr$ sea-level curve must also be taken into account in any age interpretation. For the Pliocene and Pleistocene, the curve includes sections of relatively flat gradient (2.54–4.8 Ma) and steeper gradient (<2.54 Ma and > 4.8 Ma). Where the curve is relatively flat, the error range is significantly greater (0.1–0.35 Ma) than where it is steeper (0.08–0.1 Ma). Most of the $^{87}Sr/^{86}Sr$ samples fall into the relatively flat interval and therefore provide only a broad indication of the absolute age; for example, PL03 has an age range

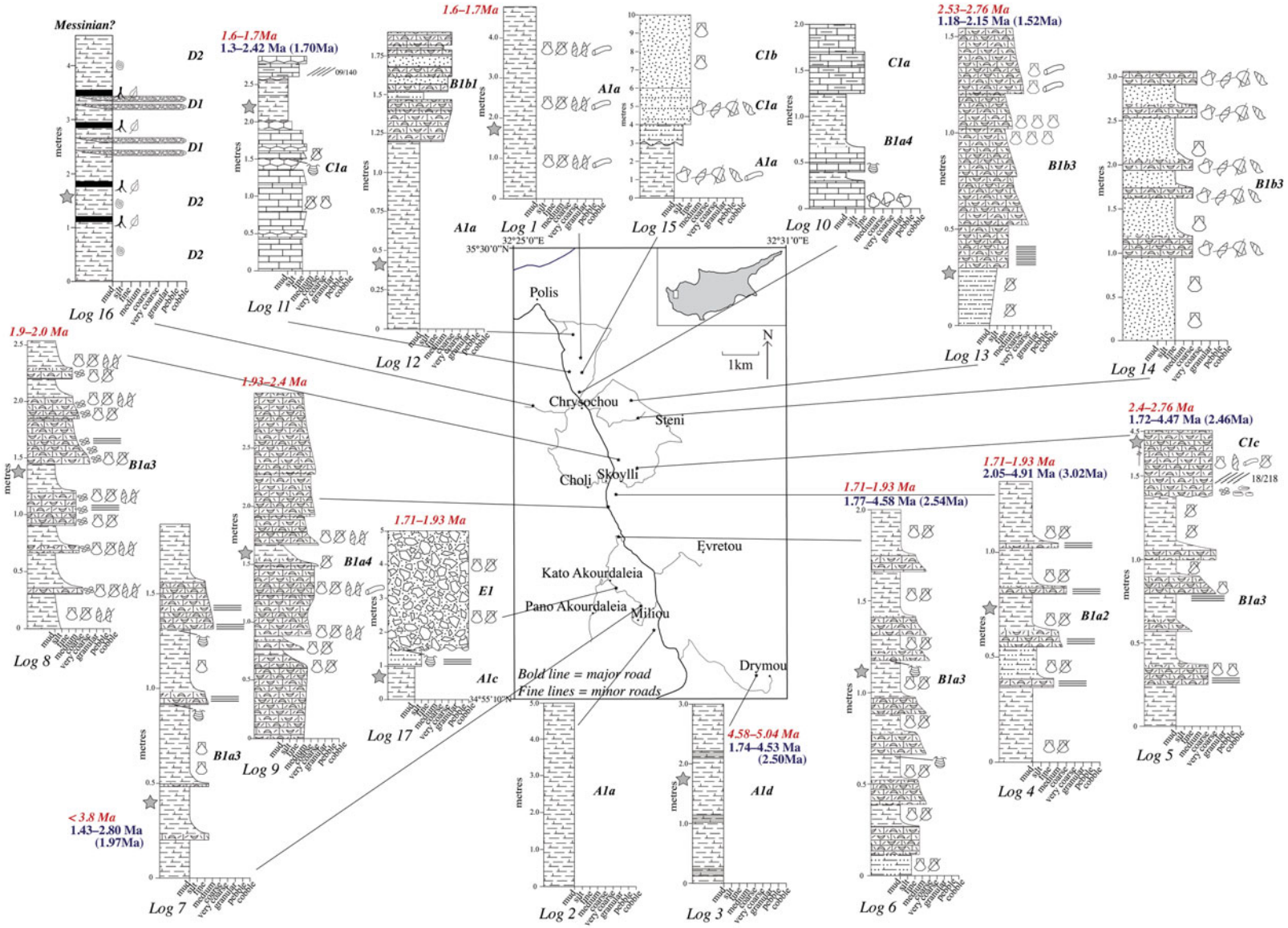

Figure 4. (Colour online) Distribution of local sections logged throughout the study area. Nannofossil age ranges are in italics (red), strontium isotopic age ranges in roman text (blue) and the assigned age given in parentheses. Most ages are within analytical error of each other; see Section 4 for further information on any discrepancies between ages. Preference is given to nannofossil ages. Stars (grey) to the left of the logs indicate the location of a dating sample. Log 16 is of an uncertain age (Messinian facies?). Facies codes are given on right-hand side of the logs as discussed in Section 6; see Table 3 for corresponding facies. Key on opposing page. Relate to Figure 3 for stratigraphy and structural details of reference map.

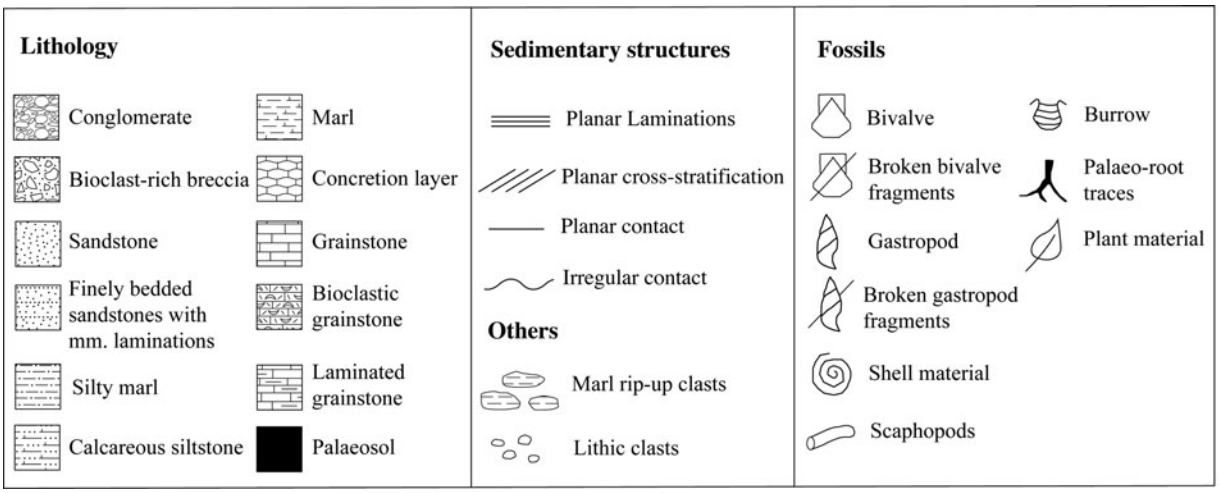

Figure 4. Continued

(including standard error) of 1.94–4.80 Ma. However, the steeper intervals of the curve allow a more accurate age determination, for example PL70 has an age range (including standard error) of 1.43–2.80 Ma. The late Pliocene – early Pleistocene $^{87}Sr/^{86}Sr$ isotopic ages have a smaller age range and, in some cases, these dates are relatively consistent with the nannofossil age ranges (e.g. sample numbers 12, 46, 65). The highest age resolution was obtained by combining the $^{87}Sr/^{86}Sr$ isotopic ages and nannofossil biochronology.

The oldest nannofossil ages (4–5.08 Ma) are in the southern part of the basin (PL35 and PL78) at low topographic levels (e.g. Fig. 4, log 3). Nannofossil ages of 2.4–3.6 Ma are generally found in and around the depocentre of the basin in the south and also towards the western and eastern flanks of the basin (e.g. Fig. 4, logs 7, 13). Nannofossil ages of 1.6 to <2.4 Ma are found near the basin axis, from Polis in the north to near Miliou in the south (e.g. Fig. 4, logs 1, 6, 11). These ages generally come from higher topographic level (south of Skoylli). Relatively early nannofossil ages are also found on the flanks, ranging from 1.81 to 5.04 Ma. Age outliers on the flanks variously range from >1.93 to <2.4 Ma and >2.76 to <3.6 Ma. In general, relatively young nannofossil ages were determined in topographically high areas (PL12, PL65, PL70 and PL74).

The oldest strontium isotopic ages (4.11 and 5.46 Ma) come from near the depositional axis, near Skoylli. Strontium isotopic ages of 2.50–3.28 Ma are recorded on the flanks of the basin and in the south of the area, from Skoylli to Polemi (i.e. Fig. 4, logs 3, 4, 6). Ages of 3.02 Ma were determined for the deeply eroded depositional axis, as exposed along the main road south of Skoylli (e.g. Fig. 4, log 4). Strontium isotopic ages over the range 1.25–2.46 Ma occur in the north of the area (e.g. Fig. 4, logs 11, 13). The same ages are also recorded in areas of higher topography in the centre of the area (south of Skoylli; e.g. Fig. 4, log 7).

5. Pliocene and Pleistocene reference succession

The combined age data indicate a general northwards younging, with the oldest samples in the south and the youngest in the north (Fig. 6). The sequences of calcareous mudstones near the depositional axis range from early Pleistocene to early Pliocene (1.93–5.08 Ma), whereas the bioclastic calcarenite–mudstone couplets in the south are dated as early Pleistocene in age (1.71–2.76 Ma). In addition, the calcareous sandstones and hemipelagic mudstones in the north are dated as early Pleistocene in age (1.6–1.7 Ma). Furthermore, some of the calcareous mudstone samples that were collected from topographically high areas in the south (e.g. PL11, PL65, PL72 and PL69) give relatively young ages, that is, early Pleistocene (1.71–2.4 Ma).

Taking into account the regional dip of the strata, the lithological correlations of the local logged sequences (Fig. 4) and the age data, an overall sedimentary succession can be inferred for the northern part of the Polis graben (north of Polemi) as shown in Figure 7. Where exposed in the south, the succession is dominated by hemipelagic mudstones *c.* 200–250 m thick, of which the base is not exposed. These fine-grained sediments pass upwards into an interval of normal-graded couplets (*c.* 100–150 m thick; see Fig. 2d), each made up of bioclastic carbonate rock fining into mudstone or siltstone. In the north, similar sediments pass upwards into calcareous sandstone, tens of metres thick with muddy intercalations (Fig. 2e). In addition, conglomerates (1–2 m thick) occur along the eastern basin margin (e.g. near Evretou dam) and calcareous breccia is exposed on the southwestern margin (2 km NW of Miliou).

5.a. Stratigraphic correlations

Comparison with the Mesaoria Basin indicates that the calcareous mudstones making up the lower part of the succession in the Polis graben are lithologically similar to the Nicosia Formation. However, additional minor

Table 1. Nannofossil biochronological results and $^{87}Sr/^{86}Sr$ isotopic data table. $^{87}Sr/^{86}Sr$ ages were obtained using Look-Up Table Version 4: 08/04 (Howarth & McArthur, 1997; McArthur, Howarth & Bailey, 2001). Samples are listed in order from north to south within the study area; samples collected on the graben flanks are indicated by [f].

Sample number (corresponding log)	Nannofossil biochronology (Ma)	$^{87}Sr/^{86}Sr$ ratio	$^{87}Sr/^{86}Sr$ age (Ma)	$^{87}Sr/^{86}Sr$ age range (error including 2×standard error) (Ma)
PL58 [f]	Barren (Messinian 'facies')			
PL59 [f]	1.93–2.4(?)			
PL02	1.7–1.93(?)	0.709122	1.25	0.86–1.61
PL51 (log 12)	Barren			
PL03 [f]	4.58–5.04	0.709064	2.78	1.94–4.80
PL05 [f]	3.0–3.6	0.709067	2.63	1.83–4.68
PL46 (log 11)	1.6–1.7	0.709095	1.70	1.3–2.42
PL42 (log 1)	1.6–1.7			
PL89 (log 13)	2.53–2.76	0.709104	1.52	1.18–2.15
PL27 [f] (log 16)	Very rare nannofossils, not diagnostic			
PL24 [f]	2.76–3.6			
PL25 [f]	1.93–2.4			
PL60 [f]	2.76–3.6			
PL96	2.53–3.6	0.709052	4.11	2.34–5.21
PL09 [f]	1.93–2.4	0.709068	2.58	1.80–4.63
PL19 (log 8)	1.9–2.0			
PL31 [f]	<3.8(?)			
PL17	Piacenzian–Gelasian transition, <3.8	0.709053	4.01	2.31–5.17
PL18 (log 5)	2.4–2.76 (Late Piacenzian or early Gelasian)	0.709071	2.46	1.72–4.47
PL35	Barren	0.709021	5.46	4.72–5.92
PL78 (log 4)	1.71–1.93(?)	0.709061	3.02	2.05–4.91
PL15	2.0–3.6	0.709061	3.02	2.05–4.91
PL61 [f]	Barren			
PL10 [f]	1.93–2.4			
PL11 [f]	1.93–2.4(?)	0.709061	3.02	2.05–4.91
PL82 (log 9)	1.93–2.4(?)			
PL74 [f]	<3.8	0.709096	1.67	1.29–2.38
PL65	1.71–1.93	0.709089	1.86	1.38–2.64
PL66 (log 6)	1.71–1.93	0.709069	2.54	1.77–4.58
PL12 [f]	2.76–3.6	0.709085	2.01	1.44–2.87
PL72 (log 17)	1.71–1.93			
PL70 (log 7)	Piacenzian or Gelasian, <3.8	0.709086	1.97	1.43–2.80
PL69	1.93–2.4			
PL20	>4.0			
PL84 (log 3)	4.58–5.04	0.70907	2.50	1.74–4.53
PL01 [f]	Rare nannofossils, not diagnostic			
PL21	4.0–5.08	0.709059	3.28	1.72–4.47
PL22	Barren (Messinian 'facies')			

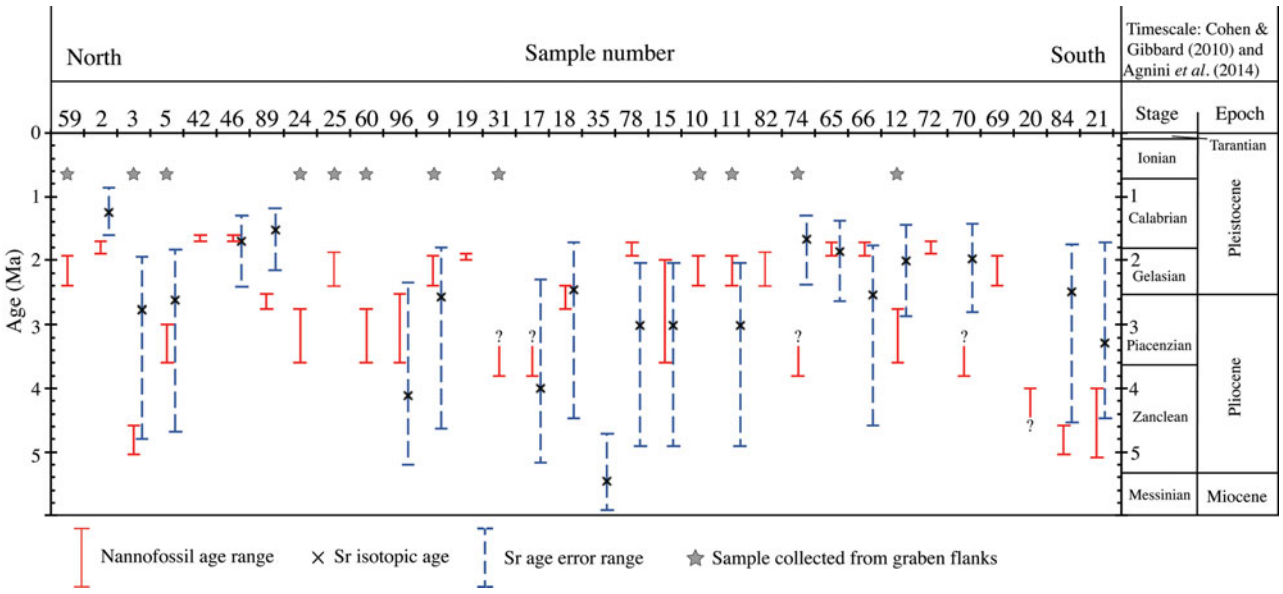

Figure 5. (Colour online) Nannofossil biochronology age ranges and $^{87}Sr/^{86}Sr$ ages with error bars (see Table 1). The ages are plotted in order from the most northerly sample to the most southerly sample. Samples collected from the graben flanks are highlighted with a star and are considered separately from samples that were collected from near the N–S-aligned basin axis. Question marks represent samples which could not be clearly dated. Timescale from Cohen & Gibbard (2010) and Agnini *et al*. (2014).

Table 2. Nannofossil biostratigraphic and biochronologic results. Samples listed from north to south across the study area as in Figure 5. Biozones and biochronology are from Backman *et al.* (2012). CNPL – Calcareous Nannofossil Pliocene. Semiquantitative abundance evaluations obtained at magnification 1200× with polarizing microscope. Total abundance: 1, *c.* 10; 2, *c.* 20; and 3, >30 specimens in a single field of view. B – barren of nannofossils. Species abundances: 0, no specimen observed; A, >1 in specimen in each field of view; AA, dominant specimens in the assemblage; C, *c.* 1 specimen in 1–10 fields of view; F, *c.* 1 specimen every 10 fields of view; R, very few specimen in > 30 fields of view; VR, 1–2 specimens observed; cf., uncertain presence.

Sample	Nannofossil total abundance	*Amaurolithus primus*	*Amaurolithus delicatus*	*Amaurolithus tricorniculatus*	*Ceratolithus rugosus*	*Calcidiscus macintyrei*	*Discoaster asymmetricus*	*Discoaster brouweri*	*Discoaster triradiatus*	*Discoaster pentaradiatus*	*Discoaster surculus*	*Discoaster tamalis*	*Discoaster variabilis*	*Helicosphaera sellii*	Small *Gephyrocapsa* spp.	Medium *Gephyrocapsa* spp.	Large *Gephyrocapsa* spp.	*Pseudoemiliania lacunosa*	*Reticulofenestra pseudoumbilicus*	*Sphenolithus* spp.	Reworked taxa	Nannofossil biostratigraphy	Nannofossil biochronology (Ma)	Chronostratigraphy
PL59	3					C		F			VR				C			A			F	CNPL6 (?)	1.93–2.4 (?)	Middle Gelasian (?)
PL02	2														C			C			C	CNPL7	1.71–1.93(?)	Gelasian–Calabrian transition
PL03	3	F	R		0			R		A	C								A	F	C	Lower CNPL2	4.58–5.04	Early Zanclean
PL05	3	0	0				R	A		F	A	F						C	0	0	C	Middle CNPL4	3.0–3.6	Piacenzian
PL46	1													R	R	R		R			F	Base CNPL8	1.6–1.7	Early Calabrian
PL42	2														C	R		R			F	Base CNPL8	1.6–1.7	Early Calabrian
PL89	2					R		R		VR	VR			R	R			F			A	Lower CNPL5	2.53–2.76	Piacenzian–Gelasian transition
PL24	3					R	F	R		R	F	C						C			F	CNPL4	2.76–3.6	Piacenzian
PL25	2					F		R						cf.				F			C	CNPL6	1.93–2.4	Gelasian
PL60	3						F	F		VR		F	R	VR				A			F	CNPL4	2.76–3.6	Piacenzian
PL96	3	VR			R		0	C		C	C	0			R			C			A	CNPL4–Lower CNPL5	2.53–3.6	Piacenzian–Gelasian transition
PL09	2																				C	CNPL6	1.93–2.4	Middle Gelasian
PL19	3					R		VR		cf.	VR	VR		F		cf.	C	A			F	Upper CNPL6	1.9–2.0	Late Gelasian
PL31	1														C			R			F	<CNPL3	<3.8 (?)	Piacenzian or Gelasian (?)
PL17	3						VR	F		F	R				R			A			F	CNPL4–CNPL5	<3.8	Piacenzian–Gelasian transition
PL18	2					R				R	VR							R			C	CNPL5	2.4–2.76	Late Piacenzian or early Gelasian
PL35	B																				R		Barren	
PL78	3					R		cf.							R			R			F	CNPL7 (?)	1.71–1.93(?)	Gelasian–Calabrian transition
PL15	2					R		VR			VR				F			C			C	CNPL4–CNPL6	2.0–3.6	Piacenzian–Gelasian
PL10	3					R	VR	VR							R			F			F	CNPL6	1.93–2.4	Gelasian
PL11	3					F	VR	VR		VR	cf.							A			C	CNPL6 (?)	1.93–2.4(?)	Gelasian (?)
PL82	3					R		0		0	0				R			R			C	CNPL6 (?)	1.93–2.4(?)	Gelasian (?)
PL74	1							VR										F			C	<CNPL3	<3.8	
PL65	2					R								F	R	cf.		C			A	CNPL7	1.71–1.93	Gelasian–Calabrian transition
PL66	2					R								0	F	cf.		R			F	CNPL7	1.71–1.93	Gelasian–Calabrian transition
PL12	3				R		R	C		F	A	R		VR				A			C	CNPL4	2.76–3.6	Piacenzian
PL72	1							VR		VR					F	R		R			F	CNPL7	1.71–1.93	Gelasian–Calabrian transition
PL70	2					F		0		0	0							R			C	<CNPL3	<3.8	Piacenzian or Gelasian
PL69	1							R						VR	F			R			F	CNPL6	1.93–2.4	Piacenzian or Gelasian
PL20	3							R cf.			R cf.			VR	F				F	F	C	CNPL1–CNPL2	>4.0	Early Pliocene
PL84	3	F	R				VR	A		AA	F									F	F	Lower CNPL2	4.58–5.04	Early Zanclean
PL21	3		VR		R	R				C	F		C						C	A	F	CNPL2	4.0–5.08	Zanclean

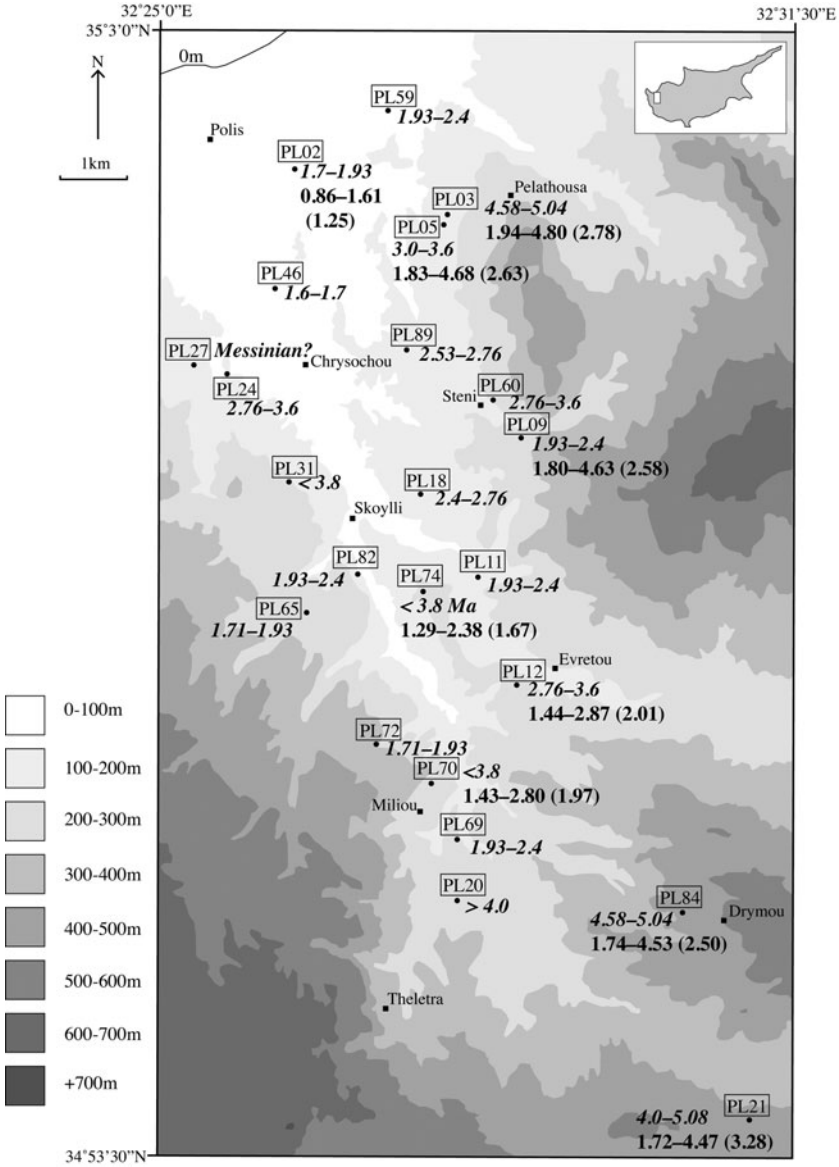

Figure 6. Shaded elevation map of the study area showing nannofossil age ranges (italics) and representative strontium isotopic age ranges (bold), with assigned ages in brackets. All ages and ranges are in Ma. Younger ages are in the north of the study area and at higher elevations. Older ages are in the south, near the basin axis and on the graben flanks.

lithologies in the Mesaoria Basin, including conglomerates of the Kakkaristra and Apalos formations, are not known to occur in the Polis graben (Henson, Browne & McGinty, 1949; Baroz, 1979; McCallum & Robertson, 1990, 1995*b*; Schirmer *et al.* 2010; Kinnaird, Robertson & Morris, 2011; Weber *et al.* 2011; Palamakumbura & Robertson, 2016). The Nicosia Formation in the Mesaoria Basin is dated as Pliocene in age based on planktonic foraminifera (Lord, Panayides & Xenophontos, 2000; Harrison *et al.* 2004).

The upwards increase in bioclastic carbonate in the lower Pleistocene part of the succession in the Polis graben is similar to the appearance of the bioclastic material in the Athalassa Formation in the Mesoaria Basin. For example, the type section at Athalassa Hill near Nicosia is dominated by shallow-water bioclastic limestones, marls and conglomerates, up to *c.* 150 m thick (Henson, Browne & McGinty, 1949). The Athalassa Formation in the Mesaoria Basin (Palamakumbura & Robertson, 2016) remains poorly dated mainly because the shallow-marine biota are not age-diagnostic. Planktonic foraminifera are also rare or reworked.

Recent work by Harrison *et al.* (2004) using borehole data in the Greater Nicosia area led to an alternative stratigraphy in which the traditional Neogene succession, including the Nicosia and the Athalassa formations, were redefined as the Nicosia Formation. Bioclastic intercalations at any level were reclassified as the Athalassa Member (reduced from formation status). This alternative stratigraphy was tested by Palamakumbura & Robertson (2016) taking account the facies evidence from northern Cyprus as a whole. These authors report a once-upwards regional change from calcareous mudstone to shallow-water bioclastic carbonates, which is consistent with

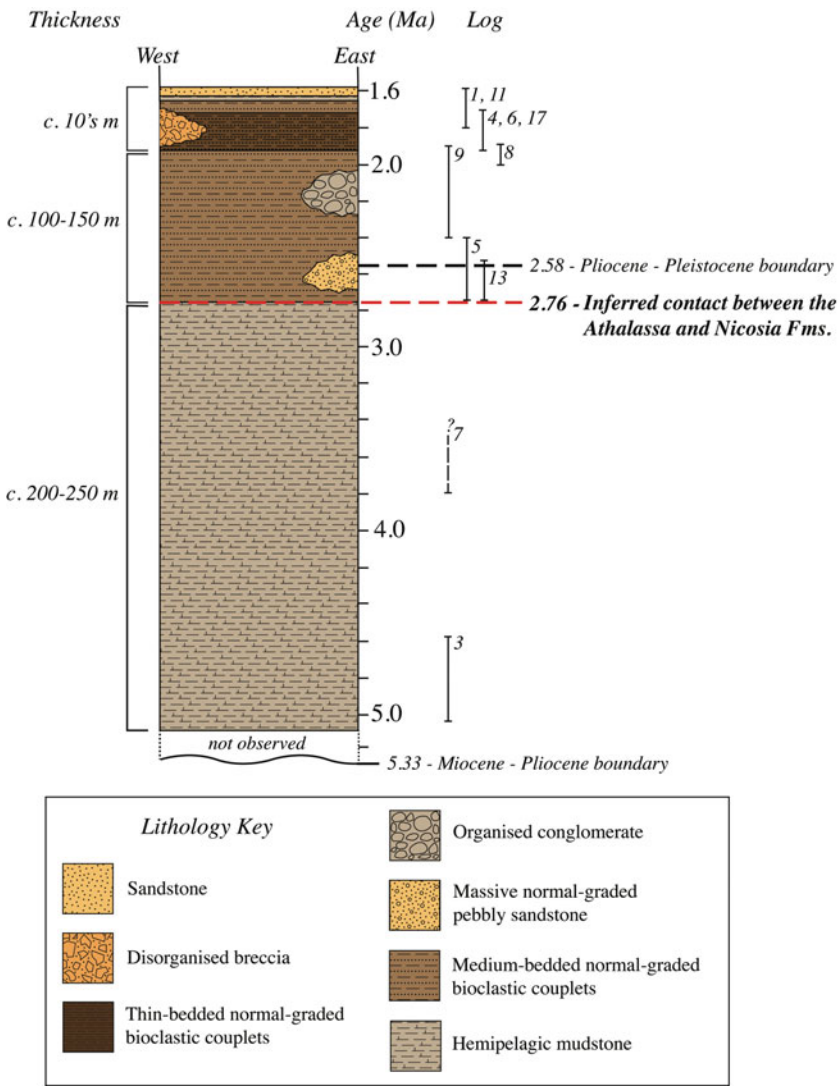

Figure 7. (Colour online) Restored sedimentary succession for the northern part of the Polis graben (north of Polemi) from late Miocene time onwards, based on a combination of regional sediment dip (and therefore topographic height), measurement of local sedimentary logs (see Fig. 4), and nannofossil and strontium isotopic age dating (see Fig. 5). The approximate positions of some of the key local logs are indicated, based on the determined nannofossil age ranges as indicated on the stratigraphic column. The dashed line (red) indicates the inferred boundary between the Athalassa and the Nicosia formations.

the traditional two-fold Nicosia–Athalassa formation stratigraphy. This stratigraphy is also retained here for the Polis graben, with the boundary between the formations being dated at *c.* 2.76 Ma.

The succession in the Mesaoria Basin is entirely shallow-marine with a preponderance of cross-bedded bioclastic packstones/grainstone. In contrast, the northern Polis graben comprises regularly bedded, normal-graded couplets of bioclastic carbonate and calcareous mudstone. The main reason for the marked facies difference is that the Polis graben represents a fault-controlled marine basin, whereas the Mesaoria Basin is interpreted an open-marine shelf or gentle ramp (Palamakumbura & Robertson, 2016).

The early Pleistocene bioclastic–mudstone couplets and calcareous sandstones making up the upper levels of the succession in the Polis graben are here correlated with the Athalassa Formation. The boundary between the two formations in the Polis graben is therefore dated at *c.* 2.76 Ma. This boundary reflects a clear lithological change between the dated lower calcareous mudstones and the upper bioclastic carbonate. The boundary between the Nicosia and Athalassa Formations is assumed to be synchronous between the Polis graben and the Mesaoria Basin mainly because the facies change is attributed to regional-scale tectonic uplift (see Section 1.a).

The definition of the Athalassa Formation adopted here has implications for the geological map of the Polis graben. The most recently published map (Constantinou, 1995) shows most of the Athalassa Formation near the northern coast of Chrysochou Bay, whereas an earlier map (Pantazis, 1979) has it extending considerably further inland, in broad agreement with our results.

In addition, a previously mapped outcrop of the Athalassa Formation along the coast west of Polis (Constantinou, 1995) was reassigned during this study to

the Pleistocene bioclastic terrace deposits, as extensively developed along the NW coast of the Akamas Peninsula (Fig. 3). The coastal area of Chrysochou Bay itself is made up of Pleistocene littoral and fluvial deposits which unconformably overlie the dated early Pleistocene calcareous sandstones and mudstones of the Athalassa Formation, as defined here (Fig. 3). There are no other candidates for the Athalassa Formation within and around the Polis graben other than the dated early Pleistocene bioclastic carbonates and interbedded mudstones and calcareous sandstones; these extend from several kilometres off the coast to *c.* 12 km inland near the basin axis.

6. Facies analysis of the Pliocene and Pleistocene sediments

The sedimentary logging combined with dating has allowed a composite sequence for the Polis graben to be recognized (Fig. 7). In the following sections, we discuss the various lithofacies present in more detail as the basis for an interpretation of the depositional processes involved.

Using the well-known facies classification of Pickering & Hiscott (2015), six lithofacies are recognized in the northern Polis graben together with nine subfacies groups (Table 3). Bed thicknesses are defined according to Ingram (1954) as thin beds (3–10 cm), medium beds (10–30 cm), thick beds (30–100 cm) and very thick beds (>100 cm). Carbonate facies, mostly calcarenite, are classified using Dunham's (1962) scheme. The representative sedimentary logs shown in the uppermost box of Figure 8 are early Pleistocene to Pliocene in age, whereas those in the lower box are Pleistocene in age.

6.a. Facies A1: hemipelagic mudstones

This facies type occurs as four subfacies, described in the following sections.

6.a.1. Subfacies A1a: structureless hemipelagic mudstone

This is mainly structureless hemipelagic mudstone which is exposed as numerous short sequences 1–5 m thick (Fig. 8, log 1; Fig. 9a). The hemipelagic mudstone ranges from light brown to dark brown with a greenish tinge. Some local sequences include calcareous siltstone, but calcareous mudstone is dominant overall. Macrofossils (e.g. pectens, gastropods and scaphopods) are commonly present, either in original life position or as reworked accumulations (i.e. death assemblages). Planktonic foraminifera are scattered throughout, especially within darker-coloured calcareous mudstone. Small numbers of benthic foraminifera were noted in some of the samples that were washed for strontium isotopic dating. Although planktonic foraminifera are generally more abundant, benthic foraminifera make up *c.* 50 % or more of the total number of foraminifera in several samples (e.g. sample numbers: 2, 18, 42, 46, 72, 74, 89).

6.a.2. Subfacies A1b: structureless hemipelagic mudstone with large macrofossils

These mudstones are structureless, brown to dark brown and contain numerous large macrofossils mostly as broken and whole oysters, pectens, scaphopods and gastropods. In road-cuts these mudstone sections are up to 10 m thick. The macrofossils, particularly oysters and scaphopods, range from <1 to *c.* 8 cm in size. In one road-cut section on the western flank of the northern graben (2 km east of Androlikou; Fig. 3), broken and whole Gryphaea (up to 10 cm long; average length 7–9 cm) are highly abundant, together with both broken and whole large pecten shells (up to 9 cm; average size 4–8 cm) and oyster shells. The macrofossils are variably interpreted as being in life position or as death assemblages (i.e. reworked accumulations). Planktonic foraminifera occur within the interbedded structureless mudstones. This subfacies is only known on the western flank of the northern graben.

6.a.3. Subfacies A1c: laminated hemipelagic mudstone

These mudstones are dark brown to light brown, finely laminated (millimetre scale), calcareous and occur in intervals of thickness up to 6 m. Planktonic foraminifera and bivalves (e.g. pectens) are characteristic, with minor amounts of benthic foraminifera.

6.a.4. Subfacies A1d: thickly bedded hemipelagic mudstone

The bedding, which ranges in thickness from 0.5 to 1.1 m, is defined by alternating light brown and dark brown calcareous mudstone. The darker brown beds are of medium thickness (10–15 cm; Fig. 8, log 3). Planktonic and benthic foraminifera are present throughout (e.g. 1 km west of Chrysochou).

6.b. Facies B1: repeated normal-graded bioclastic couplets

Two subfacies occur which are subdivided, as detailed in the following sections.

6.b.1. Subfacies B1a: organized bioclastic sandstone–mudstone couplets

This subfacies has a range of bed thicknesses:

- B1a1, thin-bedded sandstone–mudstone couplets;
- B1a2, thin-bedded sandstone to medium-bedded mudstone couplets (Fig. 8, log 4);
- B1a3, medium-bedded sandstone–mudstone couplets (Fig. 4, logs 6–8; Fig. 8, log 5); and
- B1a4, medium- to thick-bedded sandstone-mudstone couplets (Fig. 4, log 10; Fig. 8, log 9).

Subfacies B1a is commonly developed throughout the study area. It comprises repeated planar-bedded, fine- to coarse-grained bioclastic packstones and grainstones that are interbedded with structureless mudstone. The packstone and grainstone beds fine

Table 3. Summary of Pliocene and Pleistocene lithofacies and their inferred depositional environments in the northern part of the Polis graben.

Facies Code	Facies	Description	Depositional environment	Age of facies (based on nannofossil and Sr dates)
A1	**Hemipelagic mudstone**	Hemipelagic muds containing planktonic foraminifera, nannofossils and macrofossils including bivalves, gastropods, scaphopods and gryphaea	Low-energy basin	–
A1a	Structureless hemipelagic mudstone			Pliocene and Pleistocene
A1b	Structureless hemipelagic mudstone with large macrofossils			Pliocene and Pleistocene
A1c	Laminated hemipelagic mudstone			Pliocene and Pleistocene
A1d	Thickly bedded hemipelagic mudstone			Pliocene and Pleistocene
B1	**Repeated normal-graded bioclastic couplets**	Couplets composed of grainstone and packstone that fine upwards to mud or silt; the grainstones and packstones largely contain neritic bioclastic and some lithoclastic material; macrofossils are common in mud intervals	High-energy gravity flows (mass flow and turbidity currents); reworking of material from a shallow-marine setting into a hemipelagic environment	–
B1a	Organized bioclastic sand–mud couplets			–
B1a1	*Thin-bedded sand–mud couplets*			Pleistocene
B1a2	*Thin-bedded sand to medium-bedded mud couplets*			Pliocene and Pleistocene
B1a3	*Medium-bedded sand–mud couplets*			Pliocene and Pleistocene
B1a4	*Medium to thick-bedded sand–mud couplets*			Pleistocene
B1b	Organized normal–graded bioclastic sand couplets			–
B1b1	*Thin- to medium-bedded sand–silt couplets*			Pliocene (and Pleistocene)
B1b2	*Medium-bedded sand–silt couplets*			Pliocene
B1b3	*Medium-bedded coarse to fine sand couplets*			Pliocene and Pleistocene
B1b4	*Thick-bedded sand–silt couplets*			?
C1	**Sandstone**	Grainstone beds largely composed of terrigenous material and minor neritic material; bed bases contain abundant bioclastic material	Channelized mass flows flowing into a low-energy basin environment	–
C1a	Organized planar-stratified sandstones			Pleistocene
C1b	Disorganized thick-bedded sandstones			Pleistocene?
C1c	Massive normal-graded pebbly sandstones			Pleistocene
D1	**Organized conglomerate (localized)**	Clast-supported to matrix-supported conglomerate containing locally reworked chalk and carbonate clasts	Fluvial environment with material reaching the floodplain or lacustrine environment	Pleistocene and Miocene (Messinian)
D2	**Thickly bedded mud with palaeosols (restricted to margin)**	Brown palaeosols with fine rootlets and plant material, interbedded in thickly bedded silty muds; conglomerate lenses are present		Miocene (Messinian)?
E1	**Disorganized breccia (localized)**	Very poorly sorted breccia containing clasts of chalk and bioclastic grainstone with bioclastic shell material	Mass flows of collapsed basin material on flanks	Pleistocene

upwards from medium–coarse sandstone to mudstone, forming repeated couplets (Fig. 9b). Exposures generally range over 3–10 m in thickness, but some road-cut exposures exceed 20 m (e.g. south of Skoylli).

The bioclastic-rich packstones and grainstones range from poorly sorted to moderately sorted. Some beds contain bivalves, gastropods and scaphopods (up to 4–7 cm across). Bivalve shells were noted to be current-imbricated at one location near the basin axis (near Skoylli; Fig. 9c). Laminations (Fig. 9d), lithic granules (1 mm to 3 cm in size) and mud rip-up clasts (2–10 cm in size) are present at the base of some of the more poorly sorted grainstone beds (Fig. 9e–g). Sub-rounded to rounded clasts of wackestone (impure chalk) (8–40 cm in size) occur within calcareous mudstone at one locality on the eastern flank of the basin (near Steni; Fig. 9h).

The interbedded calcareous mudstones are grey, structureless and commonly contain poorly sorted bivalve fragments (e.g. pectens, gastropods). Horizontal and vertical burrows occur near the top of some individual mudstone beds, as noted on the western flanks and in the south of the northern graben (Fig. 9i). Near the basin axis (1 km NE of Skoylli) mudstone layers are laterally discontinuous on a metre scale due to scouring by a channel (Fig. 10a, b).

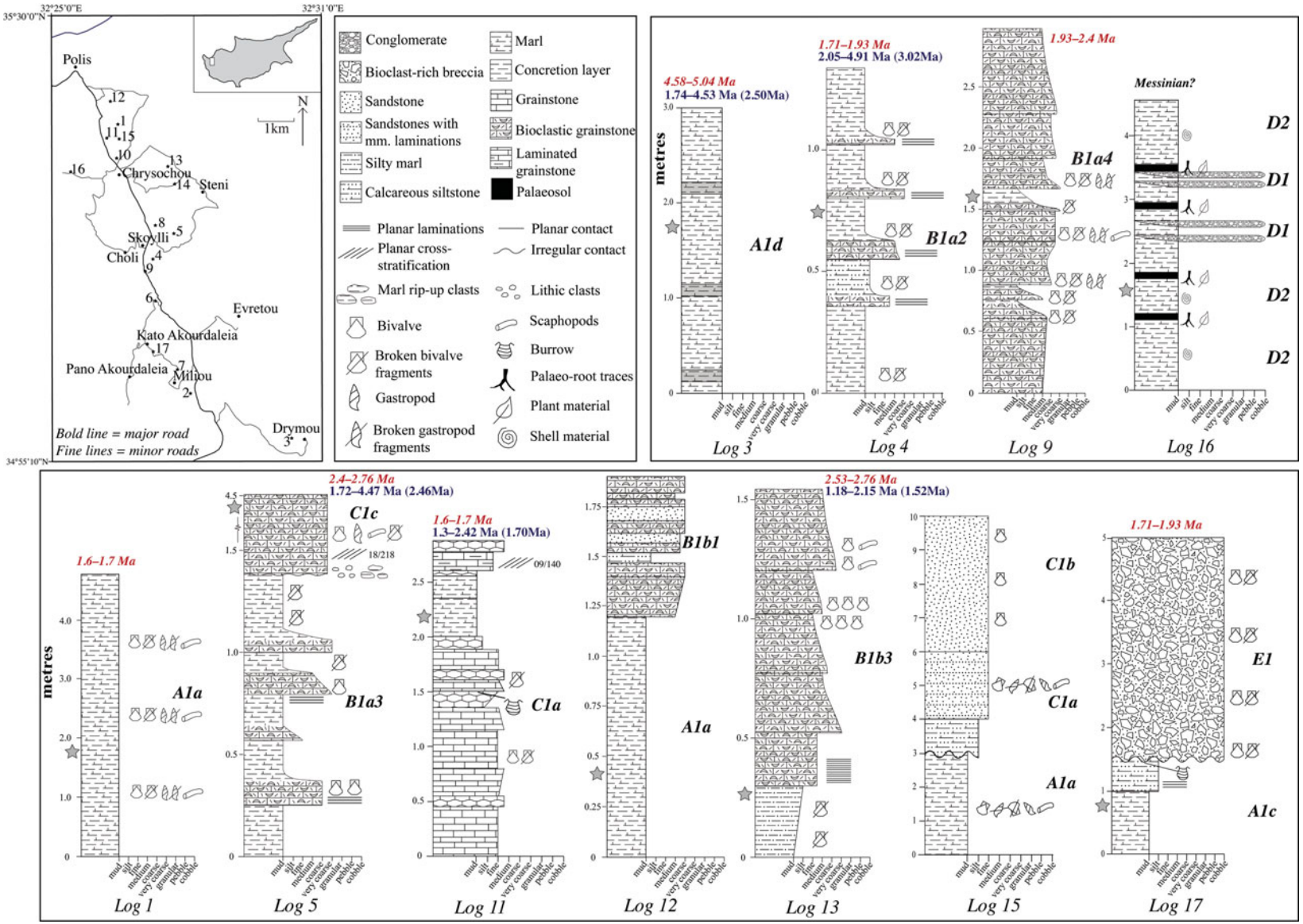

Figure 8. (Colour online) Representative sedimentary logs of the lithofacies identified within the northern Polis graben area, with locations shown on the inset map, selected from a larger number of measured logs (see Fig. 4). Facies codes are given to the right of the sedimentary logs; see Table 3 for facies classification. Beside the logs the nannofossil age ranges are given in italics (red) and the strontium isotopic age ranges in roman text (blue), with assigned ages in parentheses. Most are within analytical error of each other, see Section 4 for further information on any discrepancies between ages. Preference is given to nannofossil ages. Stars to the left of the logs indicate where samples were taken for dating.

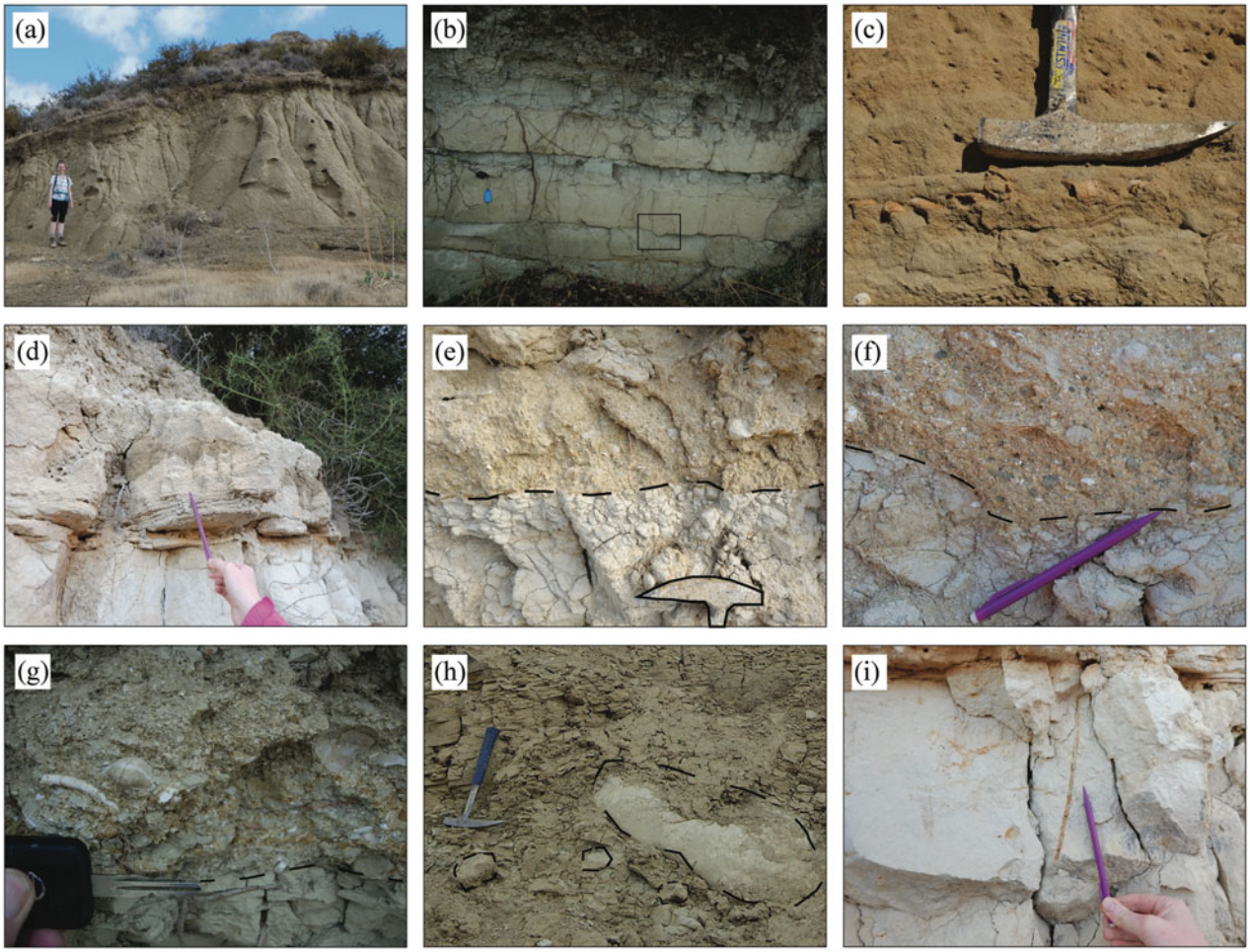

Figure 9. (Colour online) Photographs of key features of Facies A1 (hemipelagic mudstones) and Facies B1 (repeated normal-graded bioclastic couplets): (a) example of a short section of subfacies A1a (structureless hemipelagic mudstone); (b) Facies B1a3 (medium-bedded sandstone–mudstone couplets), with flute cast highlighted by box; (c) current-imbricated bivalve shells; (d) millimetre-thick laminations at the base of a grainstone bed; (e) upper part of a marl bed overlain by poorly sorted bioclast-rich grainstone; (f) lithic granules and mudstone rip-up clasts near the base of a grainstone bed; (g) very coarse-grained base of a calcarenite bed containing bivalve and scaphopod debris; (h) sub-rounded to rounded clasts of wackestone (impure chalk) within calcareous mudstone; (i) vertical and horizontal burrow traces. Hammer length: *c.* 30 cm; pencil length: *c.* 15 cm; car key length: *c.* 8 cm.

The packstone and grainstone beds are dominated by reworked bioclastic carbonate material together with minor lithoclastic material. However, some of the packstone beds are relatively lithoclast rich. Bioclastic carbonate (Fig. 11a–l) is mostly made up of echinoderms, bivalves (e.g. oysters), calcareous red algae, serpulid worm tubes, gastropods, ostracods, and both planktonic and benthic foraminifera. The planktonic foraminifera include Globigerinidae (Fig. 11g), whereas benthic foraminifera include the genera Rotaliidae and Textulariidae and species of *Eponides*, *Anomalina*, *Amphistegina*, *Neorotalia* and Miliolida (Figs 11h–l, 12j). The wackestone clasts identified are rich in planktonic foraminifera (e.g. Globigerinidae; Fig. 12a). Reworked micritic mudstone intraclasts are widespread (Fig. 12b), some of which contain reworked wackestone clasts with planktonic foraminifera (Globigerinidae) and other bioclastic carbonate material (Fig. 12c). Lithic material is mainly microcrystalline chert (Fig. 12d), basalt (Fig. 12e, f) and clinopyroxene (Fig. 12g).

6.b.2. Subfacies B1b: organized normal-graded bioclastic sandstone couplets

This subfacies occurs as a range of bed thicknesses:

- B1b1, thin to medium-bedded sandstone–siltstone couplets (Fig. 8, log 12);
- B1b2, medium-bedded sandstone–siltstone couplets;
- B1b3, medium-bedded coarse- to fine-grained sandstone couplets (Fig. 4, log 14; Fig. 8, log 13); and
- B1b4, thick-bedded sandstone–siltstone couplets.

Subfacies B1b is composed of planar-bedded bioclast-rich grainstone, interbedded with siltstone. This subfacies is common near the basin axis particularly in the south (e.g. 1 km SE of Skoylli) where the exposure is *c.* 15 m thick. Elsewhere, local exposures are up to 3 m thick. The grainstone beds are poorly sorted to moderately sorted and fine upwards into fine-grained siltstone, forming repeated couplets. The bases of the grainstone beds contain bivalve shells (up to 5 cm long), some of which are preferentially aligned,

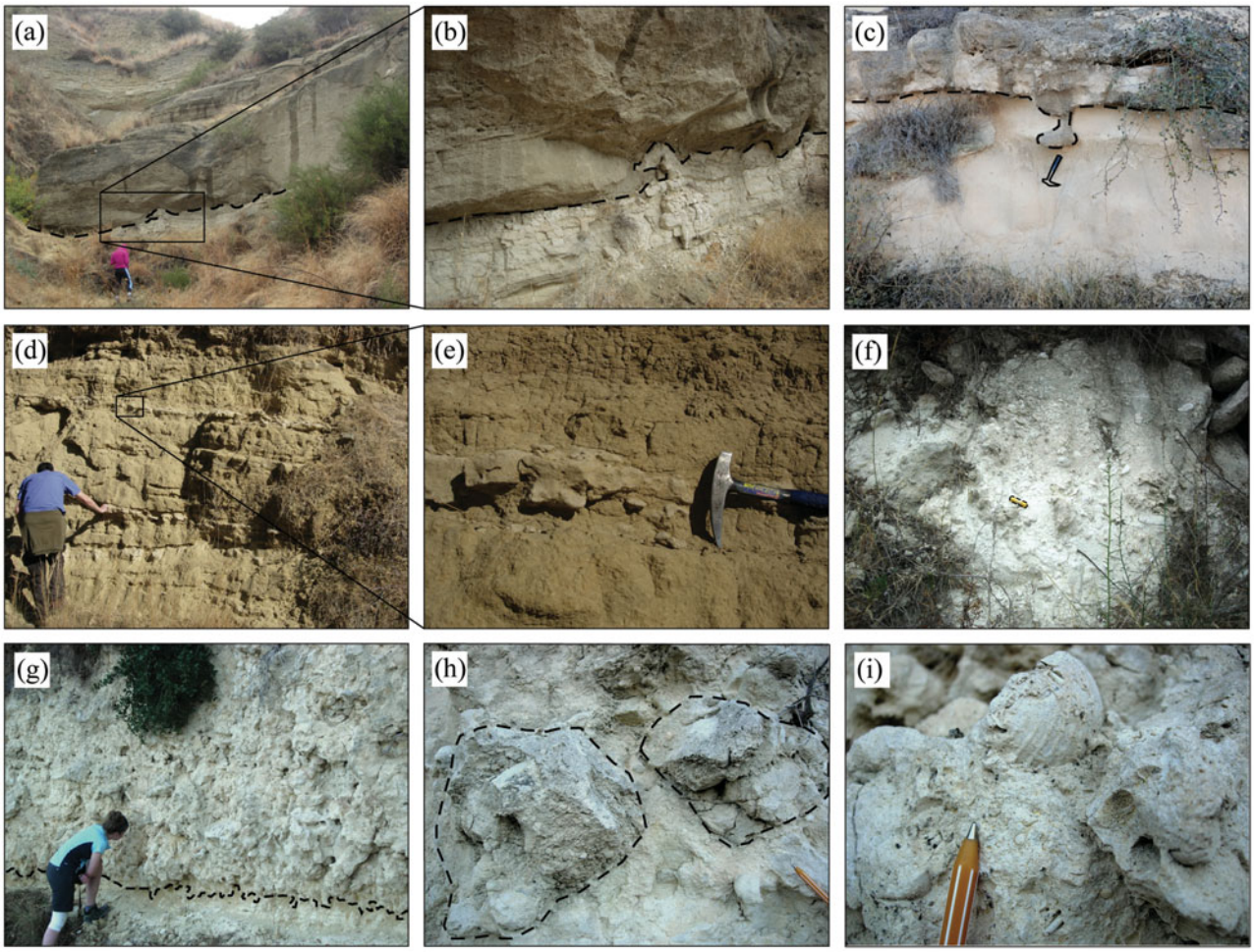

Figure 10. (Colour online) Photographs of the key features of Facies B1 (repeated normal-graded bioclastic couplets), Facies C1 (sandstones), Facies D1 (organized conglomerate) and Facies E1 (disorganized breccia). (a) Thick-bedded, down-cutting channel of subfacies C1c (massive normal-graded pebbly sandstone). (b) Scoured base of the channel downcutting into underlying subfacies B1a (bioclastic sand–mud couplets). Note the soft-sediment mobilization of the underlying marl. (c) Gutter cast eroded into marl and infilled with bioclastic carbonate. (d) Cross-stratified sandstone with cream-coloured concretionary layers. (e) Irregular concretionary layer within Facies C1 (sandstones). (f) Matrix-supported calcirudite (carbonate conglomerate) with poorly sorted clasts of reworked pelagic material within a carbonate matrix. (g) Poorly sorted carbonate breccia of Facies E1 containing bioclastic and terrigenous material, overlying subfacies A1c (laminated hemipelagic mudstones). (h) Angular clasts of reworked bioclastic grainstone within a fine to coarse-grained bioclastic-rich matrix. (i) Cemented bivalve shell present within bioclastic grainstone clast. Pen length *c.* 15 cm, hammer length: *c.* 30 cm; object length in (f): *c.* 8 cm.

and also scaphopods. Reworked microfossils appear within the matrix towards the top of individual beds. At one exposure to the east of the basin axis (1 km W of Steni), coarse to very coarse grained, poorly sorted grainstones (12–16 cm thick) contain preferentially aligned bivalves (e.g. pectens and gastropods) and microfossils. The grainstones alternate with thick-bedded (20–95 cm), structureless fine-grained sandstone beds that contain occasional bivalve shells. Vertical burrows (up to 15 cm long) are present in some siltstone layers. A flute cast was noted at the base of a bioclastic grainstone bed (Fig. 9b; 1 km SE of Skoylli).

Fine- to medium-grained bioclastic grainstones are interbedded with siltstone and fine- to medium-grained terrigenous sandstone in an exposure in the north (1 km SE of Polis). Both of these subfacies are ungraded (Fig. 8, log 12). This exposure overlies 1.2 m of subfacies A1a, structureless hemipelagic mudstone.

Thick-bedded sandstone–siltstone couplets occur locally near the axis of the basin (250 m south of Choli). A moderately sorted, structureless siltstone bed (1.2 m thick) contains bivalve fragments and is then overlain by a relatively thick (>1 m) bed of very coarse-grained bioclast-rich grainstone. The contact between the siltstone and the very coarse grainstone is undulose. A gutter cast is cut into the siltstone beneath and infilled with the coarse grainstone (Fig. 10c). The base of this bed is rich in cemented, poorly sorted bivalve shells.

The main bioclasts (Fig. 11a–f) within the grainstones are echinoderms, bivalves (e.g. oysters), calcareous red algae, serpulid worm tubes, gastropods, ostracods, planktonic foraminifera (Globigerinidae; Fig. 11g) and the benthic foraminifera (e.g. Rotaliidae, Textulariidae, *Eponides*, *Anomalina*, *Amphistegina*, *Neorotalia* and Miliolida; Fig. 11h–l). Common

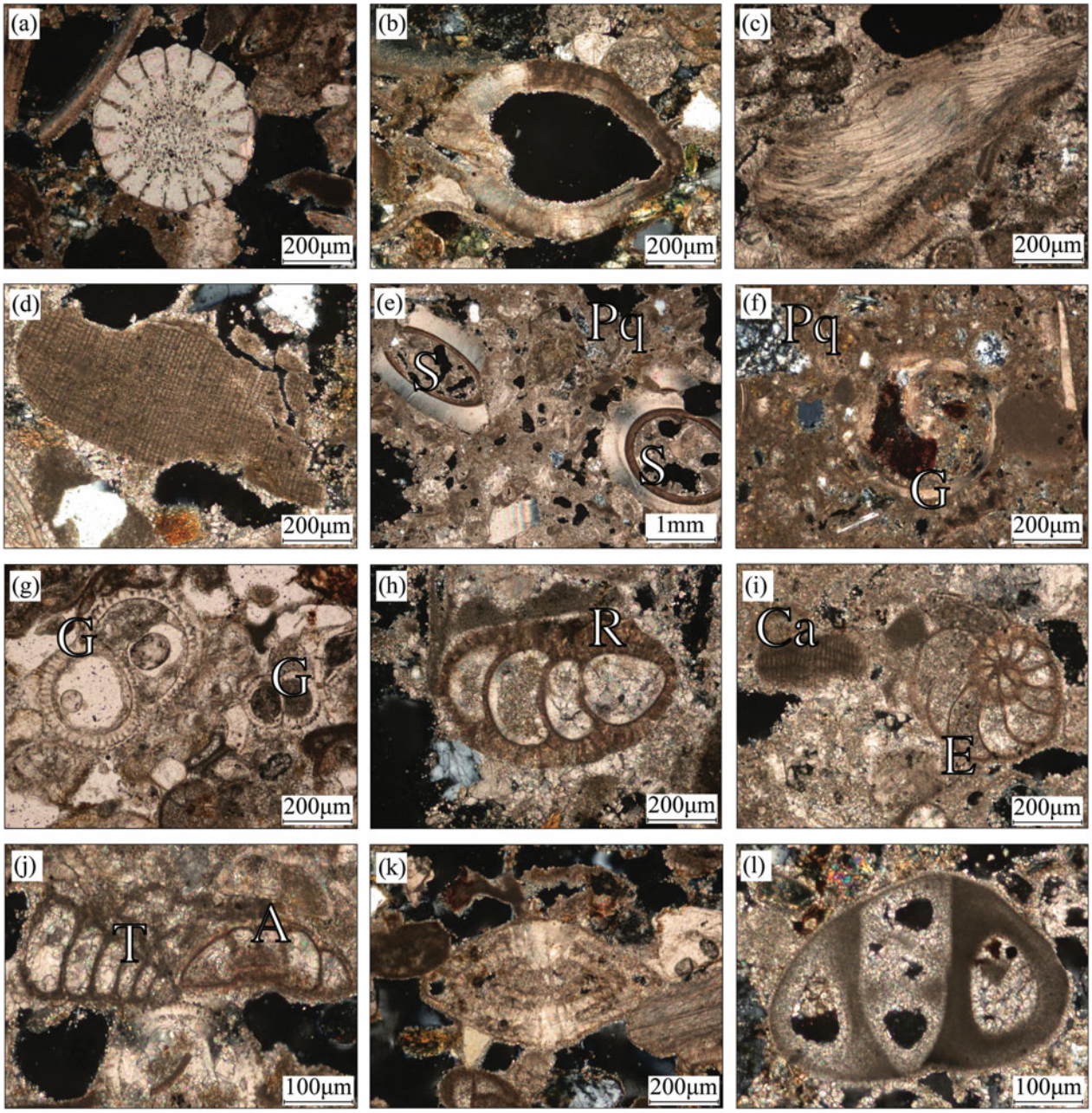

Figure 11. (Colour online) Photomicrographs of redeposited carbonate material within Facies B1 (repeated normal-graded bioclastic couplets) and Facies C1 (sandstones): (a) echinoderm spine; (b) bivalve shell; (c) fragment of oyster shell; (d) calcareous red algae; (e) serpulid worm tubes with algal growth on the inner tube (S) and also polycrystalline quartz (Pq); (f) gastropod (G) and polycrystalline quartz (Pq); (g) planktonic foraminifera; Globigerinidae (G); (h–l) Benthic foraminifera: (h) Rotaliidae (R); (i) *Eponides* (E) and calcareous red algae (Ca); (j) *Anomalina* (A) and Textulariidae (T); (k) *Amphistigina*; (l) Miliolida. All photographs taken under cross-polarized light, other than (g) which was taken under plane-polarized light.

reworked wackestone intraclasts (Fig. 12b) may contain planktonic foraminifera (Globigerinidae) and other bioclastic material (Fig. 12c). The lithic material is mostly microcrystalline chert, basalt (fresh to altered), clinopyroxene, plagioclase, quartz and diabase (altered) (Fig. 12d–i).

6.c. Facies C1: sandstone

Three subfacies are recognized as described in the following sections.

6.c.1. Subfacies C1a: organized planar-stratified sandstone

This subfacies, in which exposures range from 2–3 m to 20 m thick, is composed of yellow to brown, planar-bedded, fine- to medium-grained grainstones of thickness 10–35 cm (Fig. 4, log 10; Fig. 8, logs 11, 15). Some beds are finely laminated with scattered burrows, as noted 500 m north of Chrysochou. At a few localities in the north (e.g. 0.5–1 km north of Chrysochou), grainstones are interbedded with minor medium- to thick-bedded mudstones (10–60 cm). The mudstone beds are brown/grey and structureless, and

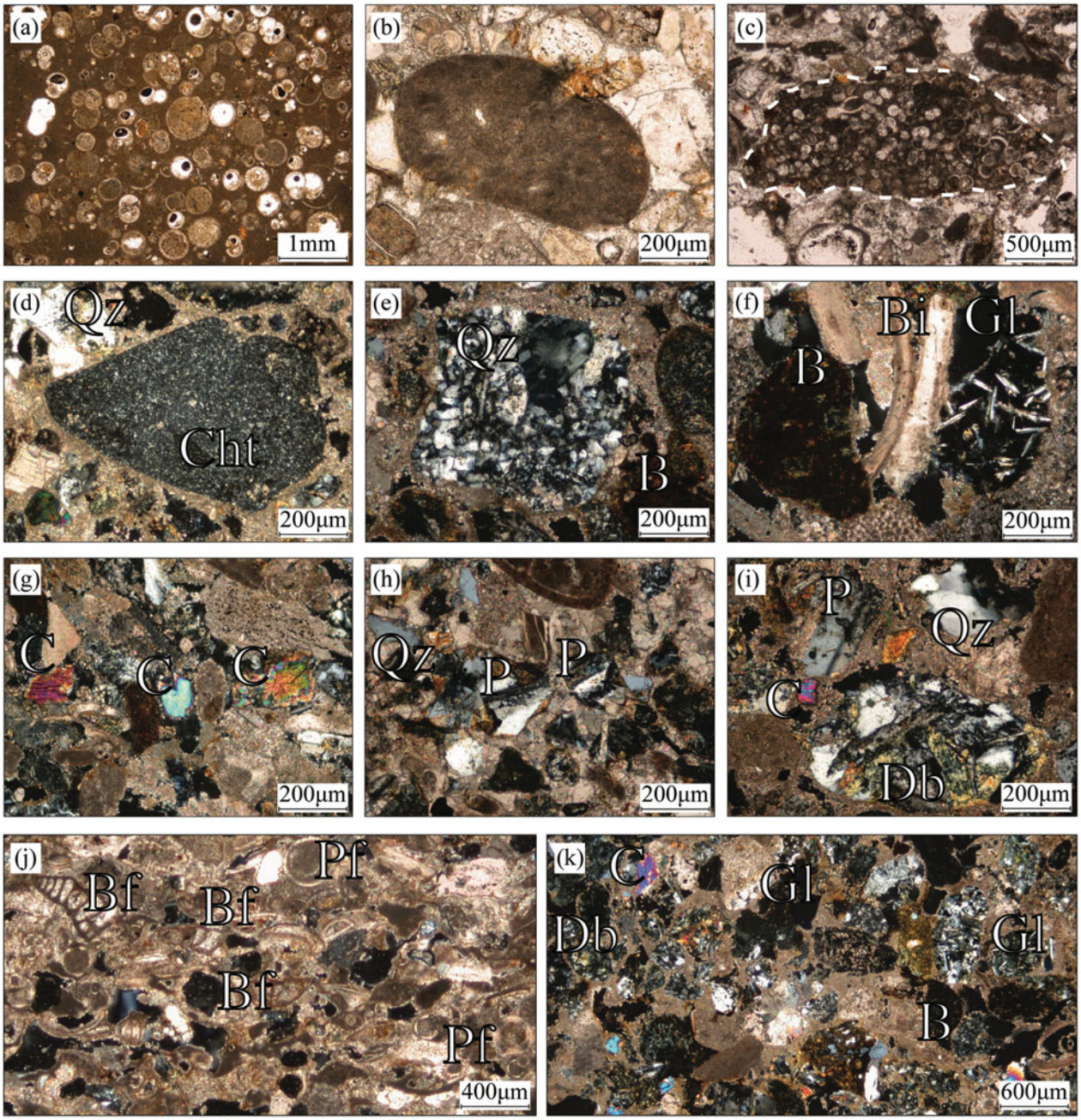

Figure 12. (Colour online) Photomicrographs of reworked carbonate and lithoclastic material within Facies B1 (repeated normal-graded bioclastic couplets) and Facies C1 (sandstones). (a) Wackestone (pelagic carbonate) with abundant planktonic foraminifera (Globigerinidae). (b) Reworked, rounded micritic intraclast in bioclastic carbonate. (c) Reworked grain of wackestone with densely packed planktonic foraminifera (suggestive of redeposition prior to reworking). (d) Sub-rounded lithoclast of microcrystalline quartzitic chert (Cht) together with a large quartz grain (Qz) in a calcareous matrix. (e) Lithoclast of quartzite with recrystallized quartz (Qz) and highly altered basalt (B) in a calcareous matrix. (f) Highly altered basalt (B), volcanic glass with micro-phenocrysts of plagioclase (Gl) and bivalve fragments (Bi) in a calcareous matrix. (g) Clinopyroxene grains (Cpx) within mainly bioclastic carbonate. (h) Plagioclase (P) and quartz grains (Qz) within a mixed siliciclastic-carbonate rock. (i) Altered diabase (Db), clinopyroxene (C), plagioclase (P) and quartz (Qz) within partly recrystallized carbonate. (j) Foraminiferal-rich grainstone of subfacies B1a3 (medium-bedded sandstone–mudstone couplets) with benthic foraminifera (Bf) and planktonic foraminifera (Pf). (k) Lithoclastic-rich subfacies C1a (organized parallel-stratified sandstone) with altered diabase (Db), altered basalt (B), clinopyroxene (C) and volcanic glass (Gl) fragments, some of which contain micro-phenocrysts of plagioclase. All photographs taken under cross-polarized light, except (b) and (c) which are under plane-polarized light.

some exposures have an undulating contact with fine sandstone above. Several medium- to thick-bedded, fine-grained grainstone beds, with mudstone interbeds, occur towards the top of the exposure as seen in the north of the basin (Fig. 8, log 11). Low-angle planar cross-bedding is present in this exposure (dipping at 9° to 140°) in which some beds are lenticular (Fig. 10d). Numerous carbonate concretions occur in this interval (Fig. 10e). Burrows are well developed at the top of the fine grainstone (Fig. 8, log 11).

North of the graben (north of Chrysochou), subfacies A1a (structureless hemipelagic mudstone) grades into 2 m of planar-stratified, medium-bedded grainstones (10–30 cm). The beds are finely laminated and contain bivalve fragments (Fig. 2e; Fig. 8, log 15). The contact between subfacies A1a (structureless hemipelagic mudstones) and the planar-stratified, medium-bedded grainstones is regular and laterally continuous.

Small exposures of subfacies A1a (structureless hemipelagic mudstone) (Fig. 9a) are scattered at different topographic levels between occurrences of subfacies C1a (organized planar-stratified sandstone). The original succession is restored as hemipelagic mud alternating with sandstones on a scale of several metres (e.g. north of Chrysochou and 1.5 km west of Chrysochou; Figs 2e, 10d; Fig. 4, log 15).

Grainstone beds in the north (north of Chrysochou) are rich in lithoclastic material together with minor carbonate grains. Basalt grains predominate (fresh, glassy basalt to altered basalt), together with minor amounts of partially recrystallized chert, clinopyroxene (augite), biotite, diabase (altered), microgabbro (rare), monocrystalline quartz and metamorphic quartzite (Fig. 12d–i, k). Bioclastic carbonate includes echinoderms, bivalve shells, calcareous red algae and reworked serpulids (Fig. 11a–e). Benthic foraminifera (*Anomalina* and Miliolida; Fig. 11j, l) and planktonic foraminifera (Globigerinidae; Fig. 11g) are present in minor amounts, together with common reworked micritic intraclasts (Fig. 12b).

6.c.2. Subfacies C1b: disorganized thick-bedded sandstone

This subfacies was identified at one exposure near the axis of the graben (1 km north of Chrysochou), where it is composed of a thick-bedded, structureless, moderately sorted, fine-grained sandstone, *c.* 4 m thick. This sandstone body contains poorly sorted oyster fragments. The exposure lies above the organized planar-stratified sandstone of subfacies C1a (Fig. 8, log 15).

6.c.3. Subfacies C1c: massive normal-graded pebbly sandstone

This subfacies was observed at only one locality (1 km NE of Skoylli), where it forms a 2–4 m thick massive bed which fines upwards from a coarse-grained, bioclastic-lithoclastic-rich, poorly sorted base to a moderately sorted, coarse to very coarse-grained sandstone top. The base of this bed exhibits a mixture of poorly sorted gastropods, scaphopods, bivalve shells (1–8 cm in length) and mudstone rip-up clasts (1–12 cm in diameter; Fig. 10a, b). The massive normal-graded pebbly sandstone repeats as a four- to five-storey stacked channel (Fig. 10a). Large-scale cross-bedding is present at the base (orientated at 18° towards 218°; Fig. 10b). The massive normal-graded pebbly sandstone is found above facies B1a3 (medium-bedded sandstone–mudstone couplets; Fig. 8, log 5).

6.d. Facies D1: organized conglomerate

Organized conglomerate was identified at two localities. The best exposure is in the SE (Evretou dam) where there is a 1–2 m thick exposure of organized conglomerate. Clasts of white pelagic carbonate (chalk) are set in a white matrix of fine-grained sandstone and gravelstone (Fig. 10f). The clasts are sub-rounded, to rounded, to elongate, and range in size from <1 cm granules to *c.* 14 cm cobbles (average size 3–7 cm). Overall, the conglomerate ranges from clast supported to matrix supported. The conglomerate is poorly sorted; however, larger clasts dominate the base and finer clasts the top of individual depositional units.

6.e. Facies E1: disorganized breccia

Disorganized breccia is only known in the SW of the graben (500 m SE of Kato Akourdaleia; Fig. 8, log 17), where it is composed of a very poorly sorted mixture of lithoclastic and bioclastic material, forming a 3.5 m thick vertical sequence (Fig. 10g). The matrix is a light orange, fine- to coarse-grained bioclastic-rich sandstone. The clasts are angular to sub-rounded, range from granules (2 mm) to large cobbles (20 cm) (average clast size: 6–10 cm); they are predominantly composed of bioclastic grainstone (Fig. 10h) and chalk (wackestone). Large vertical burrows (3–10 cm across and up to 20 cm long; Fig. 10g) extend downwards from the base of the disorganized breccia into siltstone below. Bivalve shells are present within both the bioclast-rich matrix and bioclastic grainstone clasts (1–7 cm in size; Fig. 10i). The calcareous breccia is clast- to matrix-supported throughout and occurs above subfacies A1c (laminated hemipelagic muds).

7. Discussion and interpretation

In this section we combine the new age and facies evidence to help understand the depositional and tectonic processes during the Pliocene–Pleistocene development of the Polis graben.

7.a. Sedimentary processes

The recognition of a range of different lithofacies throughout the northern Polis graben allows various depositional processes to be inferred.

Conglomerates (Facies D1: organized conglomerate) of an uncertain age (possibly Messinian) occur near the western flank of the basin in the north (e.g. 1.5 km west of Chrysochou; Fig. 4, log 16). These conglomerates are inferred to represent fluvial deposition during the Messinian period of lowered sea level. Additional sediments of an uncertain age (possibly Messinian) on the NW graben margin include thickly bedded mudstone with (reworked?) shell fragments (0.5–1.1 m thick) (Facies D2), thin dark organic-rich layers (rich in plant material) and thin conglomerates (Facies D1; Fig. 4, log 16). In addition, Pliocene

conglomerates were identified further south on the eastern flank at Evretou Dam based on nannofossil dating (Fig. 10f, PL11). These deposits represent reworking of well-rounded clasts from a nearby terrestrial setting during marine transgression of the eastern flank of the graben.

The deposition of the structureless hemipelagic mudstones (Facies A1: hemipelagic mudstones) in the lower part of the succession, near the depositional axis, reflects settling out of fine-grained sediment from the water column. Planktonic foraminifera were able to accumulate in abundance in a relatively deep-water setting (up to several hundred metres) (Fig. 7). The bivalves, gastropods and scaphopods within the hemipelagic mudstones represent a mixture of *in situ* and reworked shallow-marine carbonate material.

The normal-graded bioclastic couplets (Facies B1: repeated normal-graded bioclastic couplets) are interpreted as gravity-flow deposits. The abundance of neritic bioclastic material in sections near the basin axis (e.g. Fig. 8, log 5) indicates the existence of an adjacent shallow-water carbonate-depositing setting, although this is not preserved in the rock record. The relatively coarse, poorly sorted basal bioclastic carbonate intervals of individual beds (e.g. Fig. 9e–g) are interpreted as mass-flow deposits. In contrast, the fine-grained upper parts of the individual bioclastic beds accumulated from turbidity currents. Some of the thinner, normal-graded beds without coarse bioclastic basal material (e.g. Fig. 9b) are interpreted as entirely turbiditic.

The repetitive nature of the couplets suggests that relatively constant depositional conditions persisted for an extended time period (*c.* 2.76–1.65 Ma). The best exposed couplets near the basin axis (e.g. along the Paphos–Polis main road) exhibit laterally continuous beds of near-constant thickness and grain size over tens to hundreds of metres. These features point to accumulation on a basin plain near the basin axis. The repetitive nature of the thin-bedded couplets (e.g. 1.5 km SE of Polis; Fig. 4, log 12) is indicative of successive gravity-flow depositional events; this contrasts with other intervals where gravity-flow deposits are rare or represented by occasional, relatively thick-bedded, deposits (e.g. 750 m south of Skoylli; Fig. 4, log 9).

The lenticular calcareous sandstones (Facies C1: sandstones) that are interbedded with hemipelagic mudstone near the basin axis in the northern and the middle part of the basin are interpreted as the infill of several submarine channels (e.g. Fig. 10a, b, d). The two submarine channels that were identified are orientated NNW to SSE, indicating a possible southwesterly to westerly flow into the northern graben, sourced from the Troodos massif. The best-developed channel, located 1 km NE of Skoylli (Fig. 4, log 5), shows evidence of downcutting into underlying hemipelagic mudstones (Fig. 10b). The channel was cut and infilled by sand-sized bioclastic carbonate that accumulated by mass-flow processes. Several sandstone lenses are stacked vertically above each other (Fig. 10a), indicating that the channel remained in the same position as the basin filled. This channel may have been influenced by the presence of the major transverse fault mapped near Evretou and Sarama (Fig. 3). The bioclastic carbonate is compositionally similar to that within the couplets, and it is possible that some of the thinner and finer-grained couplets, for example *c.* 1–2 km north of Chrysochou (e.g. Fig. 4, log 10, 11, 15; Fig. 10d), could represent overbank-type deposits from additional non-exposed submarine channels.

A carbonate breccia (Facies E1: disorganized breccia) was discovered at a single locality near the western margin of the basin in the south of the area studied (near Kato Akourdaleia; Fig. 4, log 17). The poorly sorted organization and matrix-support nature of this deposit indicate formation as a debris flow. The chalky matrix and the neritic bioclastic material are likely to have been derived from the Miocene succession which is exposed at higher topographical levels on the western flank of the basin.

From the restored sedimentary succession (Fig. 7), the calculated sedimentation rate is in the range 86.2–107.7 m Ma^{-1} for the Nicosia Formation and 70.0–146.6 m Ma^{-1} for the Athalassa Formation. Corrections for compaction were not taken into account, implying that these are minimum sedimentation rates. These sedimentation rates are towards the upper end of those typical of siliciclastic shelves but towards the lower end of rates typical of deep-sea lower fan deposits (Einsele, 1992). This is consistent with sedimentation rates expected within a graben that filled with regional shelf-type deposits.

7.b. Sediment provenance

Neritic bioclastic and terrigenous clastic material are variably mixed in most of the gravity-flow deposits. The bioclastic carbonate is mostly angular and poorly sorted. In contrast, the terrigenous clastic material includes well-rounded pebbles. A relatively far-removed fluvial origin is likely for the well-rounded clasts, followed by redeposition with gravity flows.

The bioclastic material was derived from a productive shallow-marine setting. The western flank of the graben may not have been well suited as the source area; it was narrow (several kilometres) and is likely to have been swept by storms driven by prevailing westerly winds. In contrast, the eastern flank of the basin was more protected and therefore a more suitable source area. In addition, bioclastic carbonate could have been supplied from the southern termination of the basin (south of Miliou; Fig. 3), although this is outside the study area.

The redeposited facies are rich in terrigenous material (mainly Facies C1: sandstones, as exposed north of Chrysochou and near Skoylli; Fig. 4, log 5, 10, 11, 15). The composition can be compared with well-mapped outcrops around the periphery of the Polis graben (Fig. 3). The present erosion level is somewhat deeper

than it was during Pliocene time, although this is not thought to have significantly affected the source areas.

In the east, the graben is bounded by the basaltic extrusives of the Troodos ophiolite and its sedimentary cover (Fig. 3). The ophiolitic rocks are overlain by felsic volcaniclastic sediments of the Kannaviou Formation which include abundant monocrystalline (volcanic) quartz. The overlying polymict Kathikas Formation, of debris-flow origin, is a potential source of the observed terrigenous content, including quartzose sandstone, limestone, altered basalt and radiolarian chert. Stratigraphically above this, pelagic carbonates of the Lefkara Formation include diagenetically formed quartzitic chert. Significantly, the Lefkara Formation is only exposed in the southern graben area in contrast to Miocene chalks, bioclastic carbonates and reefal facies of the northern graben. A similar range of source lithologies is exposed on both flanks of the graben. However, ophiolitic extrusive rocks are much more widely exposed in the east, whereas sedimentary and igneous rocks of the Mamonia Complex are widespread in the west, including quartzose sandstone, radiolarian chert, redeposited limestone and altered basalt.

This terrigenous material (mainly Facies C1: sandstones) includes relatively unaltered basalt, basaltic glass (hyaloclastite) and clinopyroxene for which the Troodos ophiolitic extrusives, as widely exposed on the eastern margin of the basin, are the likely source. In addition, colourless, unstrained monocrystalline quartz volcanic grains, including elongate shards, are likely to have been derived from the Kannaviou Formation, which is mostly widely exposed on the eastern margin of the basin. Outcrops of the Kannaviou Formation on the western side of the basin are located west of the drainage divide and are therefore unlikely to have reached the Polis graben. Grains of highly altered (commonly chloritized) basalt could have come from the Mamonia Complex (Dhiarizos Group) directly or indirectly by recycling from the Kathikas Formation. The meta-quartzite observed in some samples could have been derived by recycling from sandstones within the Mamonia Complex (Vlambouros Formation), or instead directly from metamorphic rocks (Ayia Varvara Formation) that locally occur within the Mamonia Complex.

The Akamas Peninsula and its southerly extension formed a narrow (several kilometres) elevated lineament with limited drainage into the Polis graben. In contrast, sediment could be supplied from a much larger hinterland on the western flank of the graben. Sediment supply from beyond the southern limit of the basin is unlikely as this area (Polemi Basin) was infilled by thick Messinian evaporites that remain largely intact. In addition the Polis graben was segmented, especially by the transverse Sarama lineament (Payne & Robertson, 1995, 2000; Fig. 3), which is inferred to have influenced Pliocene sediment input including the stacked channelized sands (Facies C1: sandstones).

The incoming of bioclastic carbonate (Athalassa Foramtion) is likely to relate to tectonic uplift, as noted above, focussed on the Troodos massif which would have favoured erosion and sediment supply along the eastern margin of the Polis basin. Taken together, the evidence suggests that sediment was preferentially derived from the eastern periphery of the basin, particularly from exposures adjacent to the southeastern margin of the Polis graben.

7.c. Extensional faulting versus graben fill

Previous work on the Polis graben indicated that extensional faulting became active by the Tortonian and continued during the Messinian, with limited fault activity thereafter (Payne & Robertson, 1995, 2000). During this study, it was observed that the western flank of the northern graben is intensely faulted and downthrown (Fig. 13a), with evidence of Miocene, Pliocene and possibly Pleistocene extensional faulting (Fig. 13b, c). On the western flank, downthrow of Pliocene sediments reaches *c.* 100 m in places. For example, exposures of Facies A1 (hemipelagic mudstones) and Facies C1 (sandstones) are found 1 km north of Chrysochou at an elevation of *c.* 50 m, and are also 1.5 km west of Chrysochou at an elevation of *c.* 140 m. Facies A1 also occur 3 km west of Chrysochou at an elevation of *c.* 220 m.

On the eastern flank, the Pliocene is cut by normal faults and several small transfer faults at several localities (e.g. Fig. 13d). In support, sample PL03 (SW of Pelathousa), with a nannofossil age of 4.58–5.04 Ma, lies topographically higher than PL05; this is located *c.* 150 m to the SSW, with a nannofossil age of 3.0–3.6 Ma. The decrease in age topographically downwards confirms that down-to-the-SE normal faulting has taken place in this case (Fig. 13d, e). Rotated fault blocks of Miocene sedimentary rocks are also present. The evidence indicates that faulting continued into Pliocene time (Fig. 13f).

Overall, post-Messinian faulting appears to have been focused on the outer western flank, accentuating the overall structural asymmetry that began during late Miocene time. However, additional structural data are needed to test and develop this interpretation.

The timing of the extensional faults that cut the Pliocene sediments on both flanks is poorly constrained because of the paucity of overlying Pleistocene sediments. However, extensional faults cut dated early Pleistocene bioclastic carbonate–mudrock couplets near the basin axis, as seen along the Polis–Paphos main road south of Skoylli (e.g. Figs 5, 6, samples PL69, 70).

There are two alternatives for how the basin filled with sediments. First, if extensional faulting during and after Pliocene time formed the basin morphology, then the basal sediments exposed on the flanks of the graben should have approximately the same age as the oldest sediment in the depocentre. Secondly, if the graben was mainly formed prior to Pliocene time, the

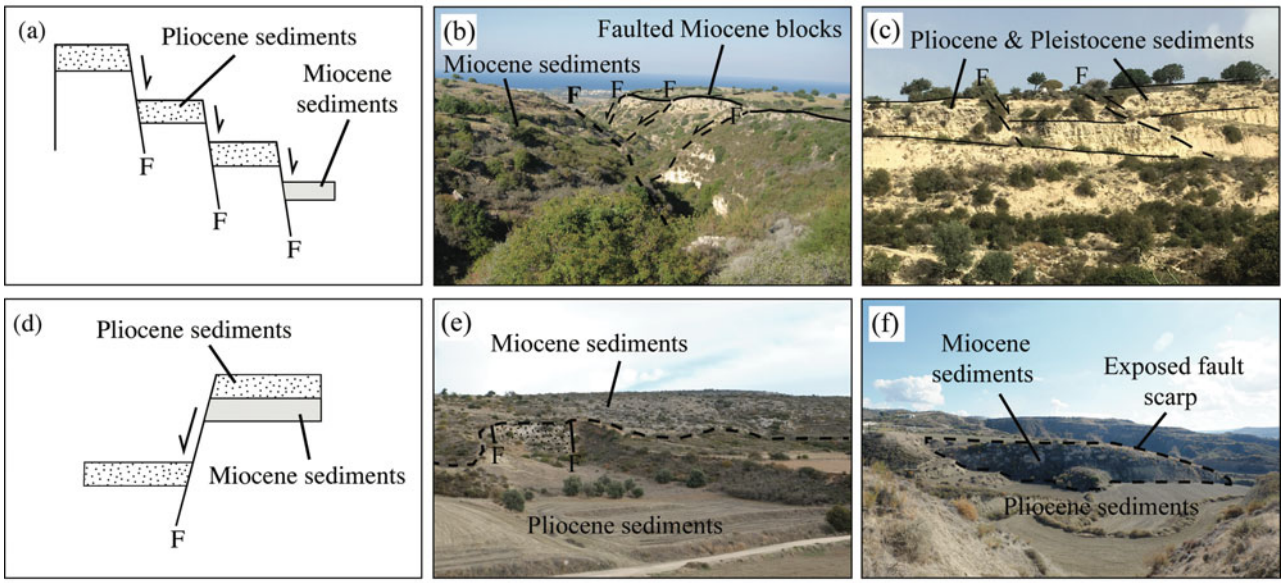

Figure 13. (Colour online) Synoptic line diagrams and photographs illustrating the extensional faulting observed on the western (a–c) and eastern (d–f) graben flank. (a) Miocene and Pliocene sediments are downthrown (by hundreds of metres) by normal faulting (western flank). (b) Down-faulted (bold) Miocene sediments (on right of photograph) subsequently underwent further extensional faulting, creating stepped Miocene fault blocks (western flank). (c) Faulted Pliocene and Pleistocene sediments on the western flank of the graben (Pleistocene age is based on lithological correlation, but requires dating for confirmation). (d) Pliocene sediments are downthrown by a normal fault exposing Miocene below (eastern flank). (e) Photograph of two extensional faults and a related fault scarp on the eastern flank of the graben, where downfaulted Pliocene sediments expose the fault scarp. (f) Pliocene sediments downthrown exposing a prominent fault scarp, highlighted by dashed line. F – faulting.

basin should have infilled with the oldest sediments in the depocentre and younger sediments at progressively higher topographic levels on the graben flanks. At Evretou dam on the eastern flank, Tortonian carbonates are cut by numerous down-to-the-west extensional faults (A. Payne, unpub. Ph.D. thesis, University of Edinburgh, 1995). Thin deposits (<10 m) of non-marine colluvium and fluvial gravel (with well-rounded clasts) there are cut by numerous small extensional faults which do not extend into the overlying Pliocene sediments (Kinnaird & Robertson, 2013). A nannofossil age of 2.76–3.6 Ma was determined within calcareous mudstone *c.* 6 m above a thin conglomerate with well-rounded clasts, which marks the local base of the Pliocene succession. This relatively young age, compared to the oldest sediments near the basin axis (e.g. 4.58–5.04 Ma; Fig. 4, log 3), is consistent with the second alternative: the basin already existed before the Pliocene, but it then took up to 2 Ma before sediment transgressed the eastern flank of the graben (at least at Evretou dam). The new results confirm that main phase of graben-forming extension took place during late Miocene time (Tortonian–Messinian) although, as noted above, significant extensional faulting continued during Pliocene–Pleistocene time. Recorded hypocentres of microearthquakes indicate that the Polis graben is currently active both onshore and in its northern extension into Chrysochou Bay (USGS online earthquake catalogue, January 2018). The overall evidence indicates that the Polis graben is still in a syn-rift stage of development.

8. Summary of Pliocene–Pleistocene basin development

A combination of pre-existing and new evidence allows the three-dimensional development of the northern Polis graben to be inferred (Fig. 14).

8.a. Early–late Pliocene (5.1–2.76 Ma)

After the Messinian salinity crisis, the pre-existing late Miocene graben began to fill with relatively deep-marine (several hundred metres) hemipelagic calcareous muds in a relatively undisturbed setting (Fig. 14a). Sediments first accumulated near the axis of the basin and then gradually expanded outwards, while the flanks of the graben remained sediment free. These deposits are equivalent to the Nicosia Formation elsewhere in Cyprus.

8.b. Late Pliocene – early Pleistocene (2.76–1.9 Ma)

A relative sea-level fall at *c.* 2.7–3.0 Ma allowed a shelly fauna to become established on the flanks of the graben, initiating the Athalassa Formation. This timing roughly corresponds to the onset of a series of large eustatic sea-level falls in response to orbital-driven Northern Hemisphere ice volume increases (Lisiecki & Raymo, 2005; Bell, Jung & Kroon, 2015). However, the sudden appearance of bioclastic carbonates and the lack of observed orbital-driven sedimentary cycles before and after the generation of abundant

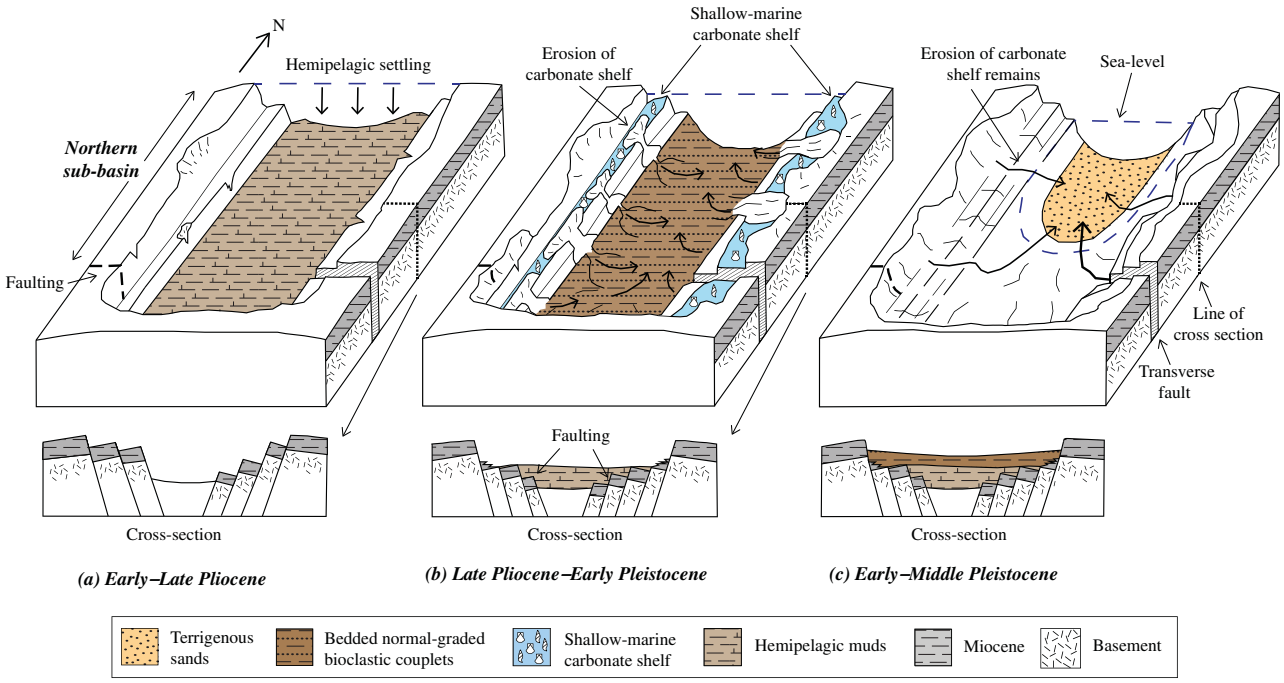

Figure 14. (Colour online) Block diagrams illustrating the generalized depositional (syn-rift) and tectonic settings of the northern part of the Polis graben during: (a) early–late Pliocene; (b) late Pliocene – early Pleistocene; and (c) early–middle Pleistocene time. No details are shown for the southern basin as it is outside the scope of research. Some sediment appears to have been redeposited from the flanks of the graben; however, the main supply is likely to have been from the SE with northwards near-axial flow within the area studied (see Fig. 15). The transverse structure influences sediment deposition, including the supply of clastic sediment. The graben morphology is adapted from A. Payne, unpub. Ph.D. thesis, University of Edinburgh, 1995.

bioclastic material suggests that the driving mechanism was tectonic uplift of the Troodos massif, centred on the Troodos massif (Mt Olympos). Mixed bioclastic-terrigenous material was then periodically transported into the basin via mass flows and turbidity currents, while calcareous hemipelagic muds continued to accumulate as background sediment (Fig. 14b).

The input of relatively coarse pebbly bioclastic sand, as observed in the SE, resulted in aggradation combined with repeated cutting and filling of submarine channels by mass-flow processes (dated at 2.4–2.76 Ma). Some of the relatively thin-bedded, fine-grained, normal-graded couplets could represent overbank deposits from more proximal submarine channels that are not exposed. In contrast, the thicker and coarser-grained, normal-graded bioclastic carbonates were probably deposited directly from a peripheral carbonate shelf, perhaps in response to slope failure or storms. Much of the clastic sediment is likely to have originated from the SE flank of the basin, followed by northwards axial transport towards the Mediterranean Sea.

8.c. Early–middle Pleistocene (1.9–1.6 Ma)

At *c.* 2–1.8 Ma, the carbonate factory on the graben flanks slowed or ceased. Detrital sediment began to infill the Polis graben as mixed carbonate-terrigenous deposits (Fig. 14c). The sediment largely accessed the basin via shallow submarine channels (several metres to tens of metres in size), as indicated by exposures in the north (north of Chrysochou) where thin-bedded terrigenous sediment of mainly Facies C1 (sandstones) were deposited (Fig. 4, logs 10, 11, 15; Fig. 10d). In addition, minor amounts of texturally immature material were locally deposited by slumping at the edge of the basin, especially on the west.

Channelized mass flows periodically flowed along the basin axis, with fine muds overstepping the channel and being deposited as overbank deposits. Such deposits were identified north of Chrysochou where Facies A1 (hemipelagic mudstones; Fig. 9a) were identified at a topographically higher level than Facies C1 (sandstones). In some logged sections hemipelagic mudstones were also found at the base of these sections (e.g. Fig. 4, logs 12, 15). Comparable channelized sands are also preserved near the highest levels of the succession as locally exposed on the upper western flank (1.5 km west of Chrysochou). This suggests that similar channelized sandstones are likely to have flooded the northern graben prior to regional emergence, although these sediments are now only locally exposed.

The terrigenous material was dominated by extrusive rock detritus from the Upper Cretaceous Troodos ophiolite, together with extrusive igneous, sedimentary and rarely metamorphic rocks from the Triassic–Cretaceous Mamonia Complex. There is additional input of a range of lithologies (e.g. volcanic quartz, chalk, diagenetic chert) from the Upper

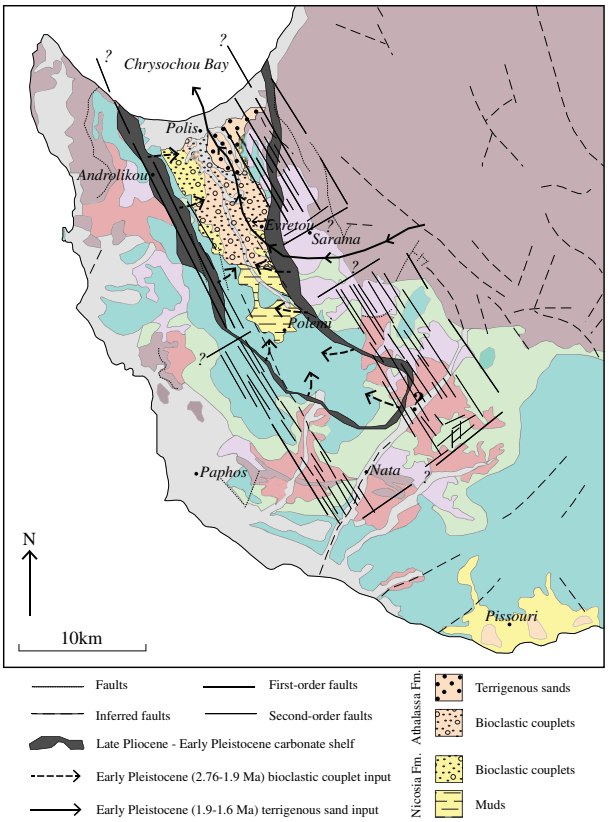

Figure 15. (Colour online) Outline palaeogeographic map of the Polis graben area with the geology of western Cyprus indicated (see Fig. 3 for corresponding ages and formations). The narrow carbonate shelf shown around the periphery of the basin and its hinterland were the source of compositionally varied sediment within the Pleistocene bioclastic couplets (dashed arrows). Late-stage Pleistocene sandstones are shown as being preferentially sourced via the transfer zone (near Sarama) (solid arrow). The faults (dotted line), inferred faults (dashed line) and geological map are adapted from the 1: 250,000 Geological Map of Cyprus, published by the Cyprus Geological Survey Department, Nicosia (Constantinou, 1995). The simplified first-order (bold line) and second-order (faint line) faults indicated are adapted from A. Payne, unpub. Ph.D. thesis, University of Edinburgh, 1995.

Cretaceous–Neogene lithologies exposed around the Polis graben. On the SW flanks of the graben, previously deposited pelagic chalk of probable Miocene age (Pakhna Formation) collapsed into the basin in the form of disorganized debris flows.

8.d. Middle Pleistocene (1.6 Ma) onwards

Sedimentation represented by the lenticular calcareous sandstones in the northern Polis graben was terminated by the onset of dramatic uplift of Cyprus as a whole, focused on the Troodos massif and the Kyrenia Range. The tectonic uplift resulted in subaerial exposure of the Polis graben. Rivers flowed radially away from the rising Troodos massif in most areas (Poole & Robertson, 1991). In western Cyprus one of the major drainage channels exploited the pre-existing structural break, marked by the major Sarama transverse fault (near Evretou dam; Fig. 15). As a result, the drainage flowed northwards along the axis of the Polis graben and cut a deep channel which was repeatedly incised and filled by conglomerates (Fig. 15; A. Poole, unpub. Ph.D. thesis, University of Edinburgh, 1992; Poole & Robertson, 2000). A fluvial to littoral to deltaic system developed just south of the present coastline of Chrysochou Bay (Poole & Robertson, 2000).

9. Conclusions

1. The Polis graben in western Cyprus provided the sedimentary accommodation space for the accumulation of a distinctive late Miocene – early Pleistocene marine succession which differs significantly from age-equivalents elsewhere in Cyprus.

2. Sedimentary logging throughout the northern Polis graben, coupled with new nannofossil and strontium isotopic dating, allows a composite succession to be erected for the basin axis.

3. Facies analysis allows the evolving palaeoenvironments to be reconstructed, ranging from Pliocene deep-marine calcareous mudstones (*c.* 5.08–2.76 Ma) to early Pleistocene (*c.* 2.76–1.6 Ma) rhythmically bedded, mixed terrigenous-bioclastic carbonate mass-flow deposits and calciturbidites (couplets), to late-stage (*c.* 1.7–1.6 Ma) terrigenous-dominated channelized sandstones.

4. Comparison of the age data and the facies evidence shows that the extensional basin was largely formed by late Miocene time and then filled progressively during Pliocene – early Pleistocene time. The flanks of the graben were transgressed by marine hemi-pelagic sediments several million years (*c.* 2.76–3.6 Ma) after post-Messinian deposition began near the basin axis.

5. Field structural evidence, combined with the nannofossil dating, indicate that extensional faulting remained active along both the western and eastern flanks of the Polis graben during Pliocene – early Pleistocene time (and probably later).

6. Taking account of the possible effects of known eustatic sea-level change, the observed incoming of bioclastic carbonates at *c.* 2.76–1.6 Ma reflects early-stage uplift of the Troodos massif further east.

7. The end of sedimentation in the basin (*c.* 1.6 Ma) is attributed to the main phase of domal uplift of the Troodos massif, centred on Mt Olympos, and uplift of Cyprus as a whole.

8. The implied two-stage (pulsed) uplift reflects ongoing early-stage collision of the African and Eurasian plates in the easternmost Mediterranean region.

Acknowledgements. The fieldwork was partly supported by the University of Edinburgh, School of GeoSciences and by the John Dixon Memorial Fund. We thank Rob Ellam, Anne Kelly and Vinnie Gallagher at the Scottish Universities Environmental Research Centre, East Kilbride for their help with the strontium isotopic dating. The first author thanks Elliot Noble for his assistance and support during

fieldwork. We also thank Romesh Palamakumbura, Gillian McCay, Torin Cannings and Eliza Calder for scientific discussion and assistance. The manuscript benefitted from comments by two anonymous referees.

Supplementary material

To view supplementary material for this article, please visit https://doi.org/10.1017/S0016756818000286

References

Agnini, C., Fornaciari, E., Raffi, I., Catanzariti, R., Pälike, H., Backman, J. & Rio, D. 2014. Biozonation and biochronology of Paleogene calcareous nannofossils from low and middle latitudes. *Newsletters on Stratigraphy* **47** (2), 131–81.

Armijo, R., Meyer, B., Hubert, A. & Barka, A. 1999. Westward propagation of the North Anatolian fault into the northern Aegean: timing and kinematics. *Geology* **27** (3), 267–70.

Backman, J., Raffi, I., Rio, D., Fornaciari, E. & Pälike, H. 2012. Biozonation and biochronology of Miocene through Pleistocene calcareous nannofossils from low and intermediate latitudes. *Newsletters on Stratigraphy* **45** (3), 221–44.

Baroz, F. 1979. Étude géologique dans le Pentadaktylos et la Mesaoria (Chypre Septentrionale). Nancy, Université de Nancy. Published thesis.

Bear, L. M. 1960. The geology and mineral resources of the Akaki-Lythrodondha area. Cyprus, Geological Survey Department, Memoir 3, 122.

Bell, D. B., Jung, S. J. A. & Kroon, D. 2015. The Plio-Pleistocene development of Atlantic deep-water circulation and its influence on climate trends. *Quaternary Science Reviews* **123**, 265–82.

Ben-Avraham, Z., Tibor, G., Limonov, A. F., Leybov, M. B., Ivanov, M. K., Tokarev, M. Y. & Woodside, J. M. 1995. Structure and tectonics of the eastern Cyprean Arc. *Marine and Petroleum Geology* **12** (3), 263–71.

Banner, F. T., Lord, A. R. & BouDagher-Fadel, M. K. 1999. The Terra Limestone Member (Miocene) of western Cyprus. *Greifswalder Geowissenschaftliche Beitrage* **6**, 503–15.

BouDagher-Fadel, M. & Lord, A. 2006. Illusory stratigraphy decoded by Oligocene-Miocene autochthonous and allochthonous foraminifera in the Terra Member, Pakhna Formation (Cyprus). *Stratigraphy* **3**(3), 217–26.

Boulton, S. J., Robertson, A. H. F., Ellam, R. M., Şafak, Ü. & Ünlügenç, U. C. 2007. Strontium isotopic and micropalaeontological dating used to help redefine the stratigraphy of the neotectonic Hatay Graben, southern Turkey. *Turkish Journal of Earth Sciences* **16** (2), 141–79.

Boulton, S. J., Robertson, A. & Ünlügenç, U. 2006. Tectonic and sedimentary evolution of the Cenozoic Hatay Graben, Southern Turkey: a two-phase model for graben formation. In *Tectonic Development of the Eastern Mediterranean Region* (eds A. H. F. Robertson & D. Mountrakis), pp. 613–34. Geological Society, London, Special Publication no. 260.

Çiftçi, N. B. & Bozkurt, E. 2009. Evolution of the Miocene sedimentary fill of the Gediz Graben, SW Turkey. *Sedimentary Geology* **216** (3), 49–79.

Civile, D., Lodolo, E., Accettella, D., Geletti, R., Ben-Avraham, Z., Deponte, M., Facchin, L., Ramella, R. & Romeo, R. 2010. The Pantelleria graben (Sicily Channel, Central Mediterranean): an example of intraplate 'passive' rift. *Tectonophysics* **490** (3), 173–83.

Cohen, K. M. & Gibbard, P. L. 2010. Global chronostratigraphical correlation table for the last 2.7 million years v.2010. Cambridge, UK: Subcommission on Quaternary Stratigraphy, International Commission on Stratigraphy.

Constantinou, G. 1995. *Geological Map of Cyprus*. Nicosia: Geological Survey of Cyprus.

DePaolo, D. J. & Ingram, B. L. 1985. High-resolution stratigraphy with strontium isotopes. *Science* **227** (4689), 938–41.

Driscoll, N. W. & Diebold, J. B. 1999. Tectonic and stratigraphic development of the eastern Caribbean: new constraints from multichannel seismic data. *Sedimentary Basins of the World* **4**, 591–626.

Dunham, R. J. 1962. Classification of carbonate rocks according to depositional textures. *American Association of Petroleum Geologists* **1** (1): 108–21.

Einsele, G. 1992. *Sedimentary Basins: Evolution, Facies, and Sedimentary Budget*. Berlin, Heidelberg: Springer-Verlag.

Elion, P. 1983. Etude structural et sédimentologique du bassin Néogene de Pissouri (Chypre). Thèse 3e cycle, Université de Paris Sud, Orsay, France. Published thesis.

Escalona, A. & Mann, P. 2011. Tectonics, basin subsidence mechanisms, and paleogeography of the Caribbean-South American plate boundary zone. *Marine and Petroleum Geology* **28** (1), 8–39.

Follows, E. J., Robertson, A. H. F. & Scoffin, T. P. 1996. Tectonic controls on Miocene reefs and related carbonate facies in Cyprus. In *Models for Carbonate Stratigraphy from Miocene Reef Complexes of the Mediterranean Regions* (eds E. K. Franseen, M. Esteban, W. C. Ward & J.-M. Rouchy), pp. 295–315. SEPM (Society for Sedimentary Geology), Concepts in Sedimentology and Paleontology no. 5.

Gass, I. G. 1960. The Geology and Mineral Resources of the Dhali area. *Cyprus Geological Survey Department, Memoir* **4**, 116.

Hall, R. 2002. Cenozoic geological and plate tectonic evolution of SE Asia and the SW Pacific: computer-based reconstructions, model and animations. *Journal of Asian Earth Sciences* **20**, 353–434.

Hardenberg, M. F. & Robertson, A. H. 2007. Sedimentology of the NW margin of the Arabian plate and the SW–NE trending Nahr El-Kabir half-graben in northern Syria during the latest Cretaceous and Cenozoic. *Sedimentary Geology* **201** (3), 231–66.

Harrison, R. W., Newell, W. L., Batihanli, H., Panayides, I., McGeehin, J. P., Mahan, S. A., Özhűr, A., Tsiolakis, E. & Necdet, M. 2004. Tectonic framework and Late Cenozoic tectonic history of the northern part of Cyprus: implications for earthquake hazards and regional tectonics. *Journal of Asian Earth Sciences* **23** (2), 191–210.

Harrison, R. W., Newell, W., Panayides, I., Stone, B., Tsiolakis, E., Necdet, M., Batihanli, H., Ozhur, A., Lord, A., Berksoy, O., Zomeni, Z. & Schindler, J. S. 2008. Bedrock Geologic Map of the Greater Lefkosia Area, Cyprus. US Geological Survey, Scientific Investigations Map 3046, scale 1:25 000, 36.

Harrison, R. W., Tsiolakis, E., Stone, B. D., Lord, A., McGeehin, J. P., Mahan, S. A. & Chirico, P. 2013. Late Pleistocene and Holocene uplift history of Cyprus: implications for active tectonics along the southern margin of the Anatolian microplate. In *Geological*

Development of the Anatolia and the Easternmost Mediterranean Region (eds A. H. F. Robertson, O. Parlak & U. C. Ünlügenç), pp. 561–84. Geological Society, London, Special Publication no. 372.

Henson, F. R. S., Browne, R. V. & McGinty, J. 1949. A synopsis of the stratigraphy and geological history of Cyprus. *Quarterly Journal of the Geological Society* **105** (1–4), 1–41.

Howarth, R. J. & McArthur, J. M. 1997. Statistics for strontium isotope stratigraphy. A Robust LOWESS fit to the marine Sr-isotope curve for 0–206 Ma, with look-up table for the derivation of numerical age. *Journal of Geology* **105**, 441–56.

Howell, A., Jackson, J., Copley, A., McKenzie, D. & Nissen, E. 2017. Subduction and vertical coastal motions in the eastern Mediterranean. *Geophysical Journal International* **211** (1), 593–620.

Ingram, R. L. 1954. Terminology for the thickness of stratification and parting units in sedimentary rocks. *Geological Society of America Bulletin* **65** (9), 937–8.

Kempler, D. 1998. The Eratosthenes Seamount: the possible spearhead of incipient continental collision in the Eastern Mediterranean. A background study in view of Leg 160 results. In *Proceedings of the Ocean Drilling Program* (eds A. H. F. Robertson, K. Emeis, C. Richter & A. Camerlengthi). Texas A & M University, College Station, Texas, Scientific Results no. 160.

Kempler, D. & Ben-Avraham, Z. 1987. The tectonic evolution of the Cyprean Arc. *Annales Tectonicae* **1**, 58–71.

Kinnaird, T. & Robertson, A. H. F. 2013. Tectonic and sedimentary response to subduction and incipient continental collision in southern Cyprus, easternmost Mediterranean region. In *Geological Development of the Anatolia and the Easternmost Mediterranean Region* (eds A. H. F. Robertson, O. Parlak & U. C. Ünlügenç), pp. 584–614. Geological Society, London, Special Publication no. 372.

Kinnaird, T. C., Robertson, A. H. & Morris, A. 2011. Timing of uplift of the Troodos Massif (Cyprus) constrained by sedimentary and magnetic polarity evidence. *Journal of the Geological Society* **168** (2), 457–70.

Lisiecki, L. E. & Raymo, M. E. 2005. A Pliocene-Pleistocene stack of 57 globally distributed benthic d18O records. *Paleoceanography* **20**, 1–17.

Lord, A. R., Panayides, E. U. & Xenophontos, C. 2000. A biochronostratigraphical framework for the Late Cretaceous–Recent circum-Troodos sedimentary sequence, Cyprus. In: *Proceedings of the Third International Conference on the Geology of the Eastern Mediterranean* (eds I. Panayides, C. Xenophonotos & J. Malpas), pp. 289–97. Nicosia: Geological Survey Department, Ministry of Agriculture and Natural Resources and Environment.

Lykousis, V., Sakellariou, D., Moretti, I. & Kaberi, H. 2007. Late Quaternary basin evolution of the Gulf of Corinth: Sequence stratigraphy, sedimentation, fault–slip and subsidence rates. *Tectonophysics* **440** (1), 29–51.

Main, C. E., Robertson, A. H. F. & Palamakumbura, R. N. 2016. Pleistocene geomorphological and sedimentary development of the Akaki River catchment (northeastern Troodos Massif) in relation to tectonic uplift versus climatic change. *International Journal of Earth Sciences* **105** (1), 463–85.

McArthur, J. M., Howarth, R. J. & Bailey, T. R. 2001. Strontium isotope stratigraphy: LOWESS Version 3. Best-fit line to the marine Sr-isotope curve for 0 to 509 Ma and accompanying look-up table for deriving numerical age. *Journal of Geology* **109**, 155–96.

McCallum, J. E. & Robertson, A. H. F. 1990. Pulsed uplift of the Troodos massif-evidence from the Plio-Pleistocene Mesaoria Basin. In *Ophiolites: Crustal Analogues. Proceedings of the International Symposium 'Troodos 1987'* (eds E. M. Moores, J. Malpas, A. Panayiotou & C. Xenophontos), pp. 217–30. Cyprus Geological Survey Department, Nicosia.

McCallum, J. E. & Robertson, A. H. F. 1995a. Late Pliocene-early Pleistocene Athalassa Formation, north central Cyprus: carbonate sand bodies in a shallow seaway between two emerging landmasses. *Terra Nova* **7** (2), 265–77.

McCallum, J. E. & Robertson, A. H. F. 1995b. Sedimentology of two fan-delta systems in the Pliocene– Pleistocene of the Mesaoria Basin, Cyprus. *Sedimentary Geology* **98** (1–4), 215–44.

McCay, G. A. & Robertson, A. H. F. 2013. Upper Miocene–Pleistocene deformation of the Girne (Kyrenia) Range and Dar Dere (Ovgos) lineaments, northern Cyprus: role in collision and tectonic escape in the easternmost Mediterranean region. In *Geological Development of the Anatolia and the Easternmost Mediterranean Region* (eds A. H. F. Robertson, O. Parlak & U. C. Ünlügenç), pp. 421–45. Geological Society, London, Special Publication no. 372.

McCay, G. A., Robertson, A. H. F., Kroon, D., Raffi, I., Ellam, R. M. & Necdet, M. 2013. Stratigraphy of Cretaceous to Lower Pliocene sediments in the northern part of Cyprus based on comparative 87Sr/86Sr isotopic, nannofossil and planktonic foraminiferal dating. *Geological Magazine* **150** (2), 333–59.

McClusky, S., Balassanian, S., Barka, A., Demir, C., Ergintav, S., Georgiev, I., Gurkan, O., Hamburger, M., Hurst, K., Kahle, H. & Kastens, K. 2000. Global positioning system constraints on plate kinematics and dynamics in the eastern Mediterranean and Caucasus. *Journal of Geophysical Research: Solid Earth* **105** (B3), 5695–719.

McNeill, L., Shillington, D. & Carter, G. 2017. Expedition 381 Scientific Prospectus: Corinth Active Rift Development. International Ocean Discovery Program. Published online October 2017, doi: 10.14379/iodp.sp.381.2017.

Ocakoğlu, N., Demirbağ, E. & Kuşçu, İ. 2004. Neotectonic structures in the area offshore of Alaçatı, Doğanbey and Kuşadası (western Turkey): evidence of strike-slip faulting in the Aegean extensional province. *Tectonophysics* **391** (1), 67–83.

Orszag-Sperber, F., Rouchy, J. M. & Elion, P. 1989. The sedimentary expression of regional tectonic events during the Miocene-Pliocene transition in the southern Cyprus basins. *Geological Magazine* **126** (3), 291–9.

Palamakumbura, R. N. & Robertson, A. H. 2016. Pliocene–Pleistocene sedimentary-tectonic development of the Mesaoria (Mesarya) Basin in an incipient, diachronous collisional setting: facies evidence from the north of Cyprus. *Geological Magazine*, published online 21 December 2016. doi: 10.1017/S0016756816001072.

Palamakumbura, R. N., Robertson, A. H. F., Kinnaird, T. C., van Calsteren, P., Kroon, D. & Tait, J. A. 2016. Quantitative dating of Pleistocene deposits of the Kyrenia Range, northern Cyprus: implications for timing rates of uplift and driving mechanisms. *Journal of the Geological Society* **73** (6), 933–48.

Pantazis, T. 1979. *Geological Map of Cyprus*. Nicosia: Geological Survey of Cyprus.

Payne, A. S. & Robertson, A. H. F. 1995. Neogene supra-subduction zone extension in the Polis graben system, west Cyprus. *Journal of the Geological Society* **152** (4), 613–28.

Payne, A. S. & Robertson, A. H. F. 2000. Structural evolution and regional significance of the Polis graben system, western Cyprus. In *Proceedings of the Third International Conference on the Geology of the Eastern Mediterranean*. Nicosia: Cyprus Geological Survey Department, 45–60.

Pickering, K. & Hiscott, R. 2015. *Deep Marine Systems: Processes, Deposits, Environments, Tectonic and Sedimentation*. Chichester, UK: John Wiley & Sons.

Poole, A. J. & Robertson, A. H. F. 1991. Quaternary uplift and sea-level change at an active plate boundary, Cyprus. *Journal of the Geological Society* **148** (5), 909–21.

Poole, A. J. & Robertson, A. H. F. 1998. Pleistocene fanglomerate deposition related to uplift of the Troodos Ophiolite, Cyprus. In: *Proceedings of the Ocean Drilling Program* (eds A. H. F. Robertson, K-C. Emeis, C. Richter & Camerlenghi,), pp. 545–66. Texas A & M University, College Station, Texas, Scientific Results no. 160.

Poole, A. J. & Robertson, A. H. F. 2000. Quaternary marine terraces and aeolianites in coastal south and west Cyprus: implications for regional uplift and sea-level change. In *Proceedings of the Third International Conference on the Geology of the Eastern Mediterranean* (ed. A. Panayiotou), pp. 105–23. Geological Survey Department, Nicosia.

Poole, A. J., Shimmield, G. B. & Robertson, A. H. F. 1990. Late Quaternary uplift of the Troodos ophiolite, Cyprus: Uranium-series dating of Pleistocene coral. *Geology* **18** (9), 894–7.

Poulos, S. E., Collins, M. B., Pattiaratchi, C., Cramp, A., Gull, W., Tsimplis, M. & Papatheodorou, G. 1996. Oceanography and sedimentation in the semi-enclosed, deep-water Gulf of Corinth (Greece). *Marine Geology* **134** (3), 213–35.

Purvis, M. & Robertson, A. 2005a. Miocene sedimentary evolution of the NE–SW-trending Selendi and Gördes Basins, W Turkey: implications for extensional processes. *Sedimentary Geology* **174** (1), 31–62.

Purvis, M. & Robertson, A. 2005b. Sedimentation of the Neogene–Recent Alaşehir (Gediz) continental graben system used to test alternative tectonic models for western (Aegean) Turkey. *Sedimentary Geology* **173** (1), 373–408.

Reiche, S., Hübscher, C. & Ehrhardt, A. 2016. The impact of salt on the late Messinian to recent tectonostratigraphic evolution of the Cyprus subduction zone. *Basin Research* **28** (5), 569–97.

Robertson, A. H. F. 1977a. Tertiary uplift history of the Troodos massif, Cyprus. *Geological Society of America Bulletin* **88** (12), 1763–72.

Robertson, A. H. F. 1977b. The Kannaviou Formation, Cyprus: volcaniclastic sedimentation of a probable late Cretaceous volcanic arc. *Journal of the Geological Society* **134**, 269–92.

Robertson, A. H. F. 1998. Tectonic significance of the Eratosthenes Seamount: a continental fragment in the process of collision with a subduction zone in the eastern Mediterranean (Ocean Drilling Program Leg 160). *Tectonophysics* **298** (1), 63–82.

Robertson, A. H. F., Kidd, R. B., Ivanov, M. K., Limonov, A. F., Woodside, J. M., Galindo-Zaldivar, J. & Nieto, L. 1995. Eratosthenes Seamount: collisional processes in the easternmost Mediterranean in relation to the Plio-Quaternary uplift of southern Cyprus. *Terra Nova* **7** (2), 254–64.

Robertson, A. H. F. & Kinnaird, T. C. 2016. Structural development of the central Kyrenia Range (north Cyprus) in its regional setting in the eastern Mediterranean region. *International Journal of Earth Sciences* **105** (1), 417–37.

Robertson, A. H. F. & Woodcock, N. H. 1979. Mamonia Complex, southwest Cyprus: Evolution and emplacement of a Mesozoic continental margin. *Geological Society of America Bulletin* **90** (7), 651–65.

Robertson, A. H. F. & Woodcock, N. H. 1986. The role of the Kyrenia Range lineament, Cyprus, in the geological evolution of the Eastern Mediterranean area. *Philosophical Transactions of the Royal Society of London. Series A, Mathematical and Physical Sciences* **317**, 141–77.

Rohais, S. & Moretti, I. 2017. Structural and stratigraphic architecture of the Corinth Rift (Greece): an integrated onshore to offshore basin-scale synthesis. In *Lithosphere Dynamics and Sedimentary Basins of the Arabian Plate and Surrounding Areas* (eds F. Roure, A. Amin, S. Khomsi & M. Al Garni), pp. 89–120. Cham: Springer International Publishing.

Rouchy, J. M., Orszag-Sperber, F., Blanc-Valleron, M. M., Pierre, C., Rivière, M., Combourieu-Nebout, N. & Panayides, I. 2001. Paleoenvironmental changes at the Messinian–Pliocene boundary in the eastern Mediterranean (southern Cyprus basins): significance of the Messinian Lago-Mare. *Sedimentary Geology* **145** (1), 93–117.

Schirmer, W., Weber, J., Bachtadse, V., BouDagher-Fadel, M., Heller, F., Lehmkuhl, F., Panayides, I. & Schirmer, U. 2010. Fluvial stacking due to plate collision and uplift during the Early Pleistocene in Cyprus. *Open Geosciences* **2** (4), 514–23.

Şengör, A. M. C., Görür, N. & Şaroğlu, F. 1985. Strike-slip faulting and related basin formation in zones of tectonic escape: Turkey as a case study. In *Strike-Slip Deformation, Basin Formation and Sedimentation* (eds K. D. Biddle & N. Christie-Blick), pp. 227–64. Society of Economic Paleontologists and Mineralogists, Special Publication no. 17.

Swarbrick, R. E. & Naylor, M. A. 1980. The Kathikas melange, SW Cyprus: late Cretaceous submarine debris flows. *Sedimentology* **27** (1), 63–78.

Swarbrick, R. E. & Robertson, A. H. F. 1980. Revised stratigraphy of the Mesozoic rocks of southern Cyprus. *Geological Magazine* **117** (6), 547–63.

Van de Weerd, A. A. & Armin, R. A. 1992. Origin and evolution of the Tertiary hydrocarbon-bearing basins in Kalimantan (Borneo), Indonesia. *AAPG American Association of Petroleum Geologists Bulletin* **76** (11), 1778–803.

Vidal, N., Klaeschen, D., Kopf, A., Docherty, C., Von Huene, R. & Krasheninnikov, V. A. 2000. Seismic images at the convergence zone from south of Cyprus to the Syrian coast, eastern Mediterranean. *Tectonophysics* **329** (1), 157–70.

Weber, J., Schirmer, W., Heller, F. & Bachtadse, V. 2011. Magnetostratigraphy of the Apalós Formation (early Pleistocene): evidence for pulsed uplift of Cyprus. *Geochemistry, Geophysics, Geosystems* **12** (1), doi: 10.1029/2010GC003193.

Yilmaz, Y., Genç, Ş., Gürer, F., Bozcu, M., Yilmaz, K., Karacik, Z., Altunkaynak, Ş. & Elmas, A. 2000. When did the Western Anatolian grabens begin to develop? In *Tectonics and Magmatism in Turkey and the Surrounding Area* (eds E. Bozkurt, J. A. Winchester & J. D. A. Piper), pp. 353–84. Geological Society, London, Special Publication no. 173.

Zitter, T. A., Woodside, J. M. & Mascle, J. 2003. The Anaximander Mountains: a clue to the tectonics of southwest Anatolia. *Geological Journal* **38** (3–4), 375–94.